Master Thesis
TVVR 26/5021

Post storm dune recovery at the Falsterbo peninsula

Melker Sennmark

Division of Water Resources Engineering
Department of Building and Environmental Technology
Lund University

Post storm dune recovery at the Falsterbo peninsula

By:
Melker Sennmark

Master Thesis

Division of Water Resources Engineering
Department of Building & Environmental Technology
Lund University
Box 118
221 00 Lund, Sweden

Cover image: Aerial photo of Falsterbo beach by Björn Almström.

Water Resources Engineering
TVVR-26/5021
ISSN 1101-9824

Lund 2026
www.tvrl.lth.se

Master Thesis
Division of Water Resources Engineering
Department of Building & Environmental Technology
Lund University

Swedish title:	Sanddyners Återhämtning efter Storm på Falsterbonäset
English title:	Post storm dune recovery at the Falsterbo peninsula
Author:	Melker Sennmark
Supervisor:	Caroline Hallin
Examiner:	Björn Almström
Language	English
Year:	2026
Keywords:	Post storm dune recovery; Aeolian sediment transport; Sand dunes; Coastal erosion; Grain size distribution;

Acknowledgements

Firstly, I would like to express my sincere gratitude to my supervisor, Dr. Caroline Hallin. Thank you for your invaluable guidance, continued support, and the expertise you shared throughout this entire project. I am grateful for your willingness to answer my questions on short notice, even offering to take time out of your vacation to provide your insights.

A special thanks goes to Åsa Wallin for granting me access to the laboratory at Geocentrum. Sifting through 134 sediment samples would not have been feasible without this equipment. I appreciate her patient guidance throughout the sifting process and her flexibility in adapting the laboratory space to accommodate my research needs.

I am also deeply grateful to my aunt and uncle Caroline and Mårten Rittfeldt for their generous hospitality. Opening your home in Skanör to me during my field sampling and topography measurement campaigns made the practical aspects of this work so much easier. Thank you for taking care of me and for keeping me well fed with delicious meals after long days.

Finally, my deepest gratitude belongs to my partner Julia. Your constant support, patience, and encouragement have been vital to the completion of this project. I am grateful for the sacrifices you have made to allow me the time and focus required to write this thesis.

Abstract

The southern coastline of the Falsterbo peninsula relies entirely on natural sand dunes as defense against coastal flooding. In October 2023, storm Babet caused severe dune erosion, consequently weakening the dunes protective ability. This thesis analyzes the post storm recovery of these dunes via aeolian sediment transport and investigates the underlying factors driving spatial variations in recovery along the beaches of Falsterbo, Ljunghusen, and Kämpinge. The methodology includes GNSS topographic surveys across 36 cross shore transects, GIS analysis of historical changes in vegetation line and beach width. Sediment samples were collected to determine the spatial grain size distribution. The results show an average of 53% of the eroded volume naturally returning by March 2026. The recovery rates have significant spatial variability with the highest accretion at Falsterbo in the west and the lowest at Kämpinge beach in the east. The vegetation line analysis reveals that a long term trend of shoreline progradation halted around 2012 and retreated drastically after the storm Babet. The investigation into these underlying factors revealed that finer median grain size (D50) in the swash zone correlates significantly with higher dune growth but it cannot fully explain the large spatial variability between the beaches. Other variables, such as beach width and median grain size in the dune toe showed weaker statistical correlations, indicating that natural recovery is a complex process driven by parameters not fully captured in this study. The study concludes that the natural recovery rate leaves the peninsula vulnerable to future storms and highlights the necessity for active coastal management.

Sammanfattning

Falsterbonäsets södra kustlinje är starkt beroende av sanddyner som naturligt översvämningsskydd. I oktober 2023 orsakade stormen Babet omfattande erosion på dessa dyner. Studien syftar till att analysera sanddynernas naturliga återhämtning genom eolisk sedimenttransport och undersöka vilka faktorer som driver spatiala variationer längs stränderna i Falsterbo, Ljunghusen och Kämpinge. Metodiken kombinerar topografiska GNSS-mätningar över 36 transekter, GIS-analys av historiska förändringar i vegetationslinje och strandbredd, samt provtagning av sediment för kornstorleksanalys. Resultaten visar att i genomsnitt 53 % av den eroderade volymen har återhämtat sig fram till mars 2026. Den påtagliga utmaningen är dock den stora spatiala variationen i återhämtning. Falsterbo strand i väster uppvisade högst återhämtning, medan Kämpinge i öster hade lägst, och vissa specifika avsnitt har knappt återhämtat sig alls. Eftersom dynerna fungerar som en sammanhängande skyddsvall medför dessa lokala avvikelser att det bildas svaga punkter i översvämningsskyddet. Analys av vegetationslinjerna indikerar dessutom att en lång historisk trend av tillväxt mot havet avstannade runt 2012, vilket följdes av en stor tillbakadragning efter stormen Babet. Korrelationsanalysen påvisade ett statistiskt signifikant samband där finare sand (D50) i svallzonen korrelerade med en högre grad av dyntillväxt. Dock kan denna faktor ensam inte förklara den stora spatiala variationen mellan stränderna, och andra undersökta variabler som strandbredd visade endast på svaga eller lokala samband. Sammanfattningsvis konstateras att även om dynsystemet som helhet återhämtar sig, gör de stora spatiala variationerna att skyddet riskerar att bli opålitligt vid nästa extremväder. Detta belyser ett behov för kustförvaltningen att införa en regelbunden övervakning för att identifiera när delar av kusten eroderar förbi kritiska nivåer. Aktiva åtgärder, såsom sandfodring på specifika punkter kommer troligtvis att bli nödvändiga på sikt för att bygga bort de svaga länkarna och upprätthålla översvämningsskyddet på Falsterbonäset.

Table of contents

1 Introduction

1.1 Background

From a coastal engineering perspective, the Falsterbo peninsula in southwestern Sweden is characterized by a predominantly low lying topography that is highly exposed to the dynamic weather conditions of the Baltic Sea. Extreme weather events in the Baltic basin create storm surges, resulting in temporary elevated water levels. At a calculated sea level of +2.0 meters (RH2000), almost the entire Falsterbo peninsula would be inundated, exposing thousands of residential buildings and critical infrastructure, such as healthcare facilities, schools and the peninsulas only road connecting it to the mainland to severe flooding (Länsstyrelsen Skåne, 2021). To address these vulnerabilities, Vellinge municipality initiated a flood mitigation program leading to the construction of a dike and wall system with a height of +3.0 m (RH2000). The southern coastlines of Falsterbo, Ljunghusen, and Kämpinge will remain without dikes or walls, instead they rely entirely on the natural sand dunes to constitute the defensive line and to protect against coastal erosion and flooding (Vellinge kommun, 2025). In Figure 1.1 a map of the Falsterbo peninsula and the location of the dikes, walls and sand dunes can be seen. Due to projected future sea level rise and more frequent storm surges, understanding and maintaining the protective capacity of these sand dunes is vital for coastal management in the region.

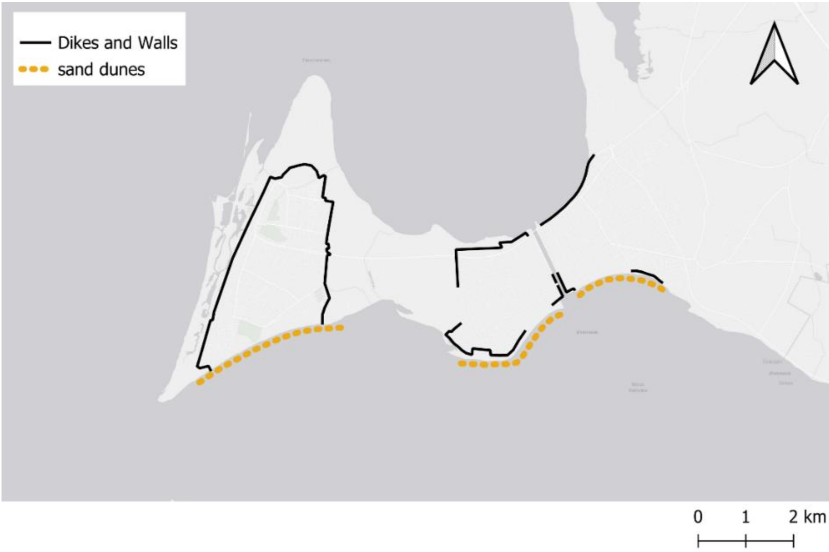

Figure 1.1: Map of the Falsterbo peninsula displaying the coastal defense. The solid black lines represent the dike and wall system. Yellow dashed lines represent the sand dunes that are studied in this thesis.

In order to effectively maintain the dunes, it is necessary to understand the natural processes taking place and shaping the dune morphology, specifically their ability to naturally recover and rebuild after a severe storm erosion event.

In October 2023, the storm Babet caused extensive dune erosion along the Falsterbo coast. The loss of dune volume ultimately meant that the municipality's protection against storm surge flooding was weakened. While dunes normally recover to some extent of their original volume naturally, the rate of recovery and whether these dunes will fully regain their pre-storm volume to provide the same protection remains unknown. The storm therefore provided an opportunity by creating a baseline to measure the rate and spatial variability of aeolian dune recovery across different sections of the peninsula, to better understand how this system responds to storm events.

1.2 Research Questions

The primary objective of this thesis is to analyze the post storm recovery of the sand dunes along the southern coast of the Falsterbo peninsula. Specifically, this study investigates the underlying factors driving spatial variations in dune volume recovery by aeolian sediment transport. This is done by evaluating the correlation between the sediment grain size, eroded sediment volume, changes in vegetation line and beach width with the dune sediment volume recovered after 2023.

To achieve this objective, the following research questions are investigated:

- To what extent has the dune volume in the Falsterbo peninsula recovered?
    - What volume of sediment was eroded during the storm Babet across the measured transects and what volume has returned at the point of measuring (March 2026)?
    - Does the rate of dune recovery differ along the peninsula's southern coast?

- How is post-storm dune recovery in Falsterbo peninsula influenced by the local beach characteristics?
    - How has the vegetation line changed historically since 1939 and how did it respond to the 2023 storm event?
    - What is the correlation between grain size and the recovery of dune volume by aeolian sediment transport?
    - How does the historical change in vegetation line correlate with dune volume recovery?
    - What is the correlation between beach width and dune volume recovery?

2 Coastal Processes

2.1 Sand Dune Morphology

Coastal foredunes are broadly defined as shore parallel, vegetated, ridges of sand situated on the uppermost beach. They generally develop through the deposition of aeolian sand within vegetation (Hesp, 2002). The morphology of a dune system is determined by the balance of eroding and accumulating processes. Dune erosion primarily occurs during storm events when elevated total water levels allow wave swash to reach the foredune. The waves erode sediment from the dune toe and transports it seaward. This process results in a steep dune face, known as a dune scarp, between the dune crest and toe (Burvingt and Castelle, 2023). Recovery and accumulation occur when a series of physical criteria are met, among others when wind direction is favorable and wind speed is higher than the threshold set by the sediment supply on the beach surface. The accretion is also dependent on vegetation and local topography which increases surface roughness, reduces wind speed and forces the sediment to deposit (Moore et al., 2025). According to Cohn et al. (2018), marine processes can also contribute to foredune growth in some cases. During elevated water levels, wave swash can deposit sediment directly onto the lower dune, instead of having a strictly erosive effect. However, marine processes are estimated to only account for between 9% and 38% of annual dune growth.

A cross shore profile reveals distinct areas with different sediment transport processes: The swash zone, the mid-beach, the dune toe, and the dune crest (shown in figure 2.1). The dune toe represents the morphological boundary between the beach and dunes.

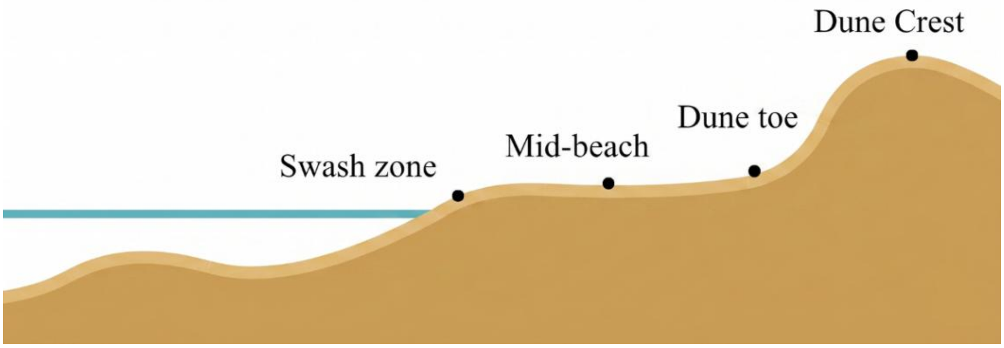

Figure 2.1: Conceptual cross shore profile illustrating specific morphological zones. The blue line represents the mean sea level.

As pioneer plant species naturally colonize the boundary where overwash is infrequent (Moore et al., 2025), the vegetation line along the coast is commonly used as a functional proxy for the dune toe position (Michałowska and Głowienka, 2022). Mapping the vegetation line from multiple consecutive years can therefore provide information on the long term foredune movement and trend. A prograding vegetation line Indicates that the accumulating process dominates, while a retreating vegetation line indicates that the erosive processes dominate.

2.2 Aeolian Sediment Transport

The growth and post-storm recovery of sand dunes depend primarily on aeolian (wind-driven) sediment transport (Cohn et al., 2018). The initiation of aeolian sediment transport depends on the balance between the aerodynamic driving forces (drag and lift) and retarding forces, primarily gravity and cohesion between particles. The driving forces are functions of the wind shear acting on the surface and in extension the wind velocity. Particle movement only begins when the threshold velocity is reached, which is the minimum velocity required for the aerodynamic forces to overcome the retarding forces (Shao, 2009). However, actual transport can be limited due to factors such as beach slope, beach width, sediment availability, soil moisture, snow and ice-cover (Fredriksson et al., 2017).

Once the threshold velocity is exceeded, aeolian sediment transport occurs through three mechanisms depending on particle size and wind conditions: suspension, saltation, and creep. Sand grains travel primarily via saltation, moving in a series of bouncing trajectories along the surface. Larger and heavier particles that cannot be lifted undergo creep, where they are pushed or rolled along the surface by the wind or by the impact of saltating grains. (Bagnold, 1941; Shao, 2009)

Coastal sand dune growth relies on a positive feedback loop between aeolian sand transport and vegetation, where vegetation causes the aeolian transported sand to deposit and the deposited sand causes new vegetation growth. The deposition of sediment due to vegetation can be explained firstly by the dissipation of wind energy due to a boundary layer forming around the vegetation which causes wind velocity to decrease below the critical threshold. Secondly, sand deposition can happen when moving particles hit the vegetation surface. Elevated topography induces similar effects on sand deposition. (Moore et al., 2025)

As aeolian transport tend to mostly transport the smaller grain sizes from the sediment supply on the beach, a grain size sorting effect in cross shore direction is commonly observed, as the larger grain sizes, with higher threshold velocity, remain on the mid-beach and the finer sediment are transported downwind and deposited on the dune (Bagnold, 1941; Hoonhout and Vries, 2016). A study by (Fredriksson et al., 2017) indicate that the favorable sediment grain size for dune building by aeolian transport is about 0.15 to 0.25 mm (D50) based on sediment sampling and analysis from Ängelholm beach.

3 Description of Study Area

3.1 The Falsterbo peninsula

The study area is the Falsterbo peninsula, located in Vellinge municipality in southwestern Scania (Skåne), Sweden. The southern coast of the peninsula is a highly dynamic morphological environment exposed to the Baltic Sea. Along this stretch, sand dunes act as a barrier providing the built environment inland and vulnerable natural habitats against coastal erosion and storm induced flooding. A map of the study area is presented in figure 3.1.

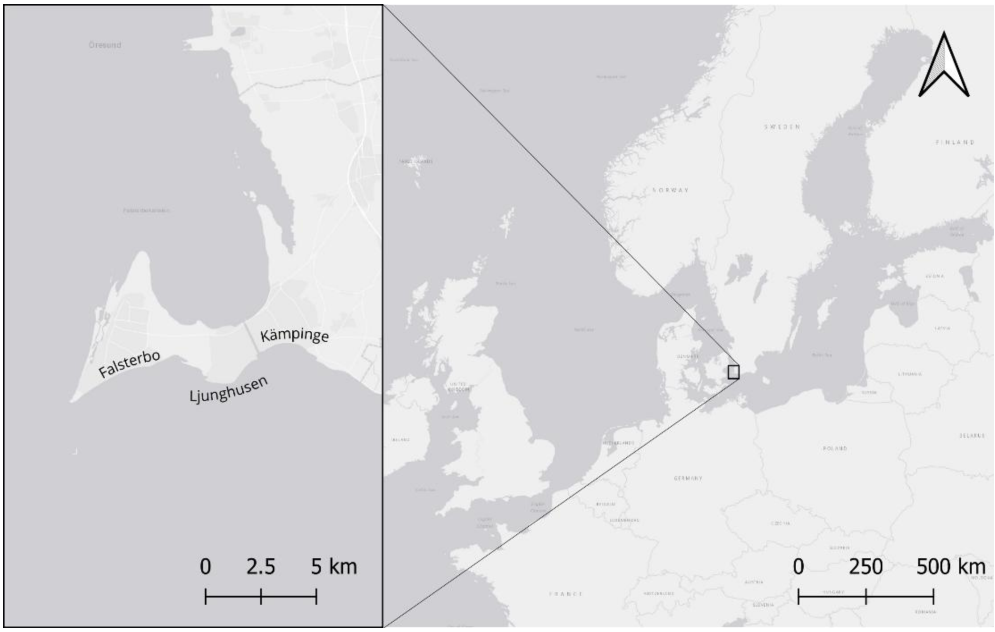

Figure 3.1: Map of the study area at the Falsterbo peninsula in southwestern Scania (Skåne), Sweden.

The investigated coastline is divided into three distinct beaches: Falsterbo, Ljunghusen, and Kämpinge beach. These shorelines differ in their geographical orientation but are also influenced by human interventions such as the Falsterbo canal breakwaters constructed in 1940, which intersect the coastline between Ljunghusen and Kämpinge. Arial photos from Falsterbo beach are presented in figure 3.2.

(a)

(b)

Figure 3.2: Aerial photographs of Falsterbo beach. (a) facing west and (b) east. (Photo: Björn Almström)

In this study, a total of 36 already established cross shore transects along the shoreline were used to analyze the spatial variation in dune recovery (as illustrated in Figure 3.3). The transects are categorized by their respective beaches and numbered from west to east:

- (F01-F19): Falsterbo beach.
- (L01-L18): Ljunghusen beach.
- (K01-K08): Kämpinge beach.

All topographical GNSS measurements, sediment sampling, and vegetation line digitization presented in this thesis are related to these specific transect lines.

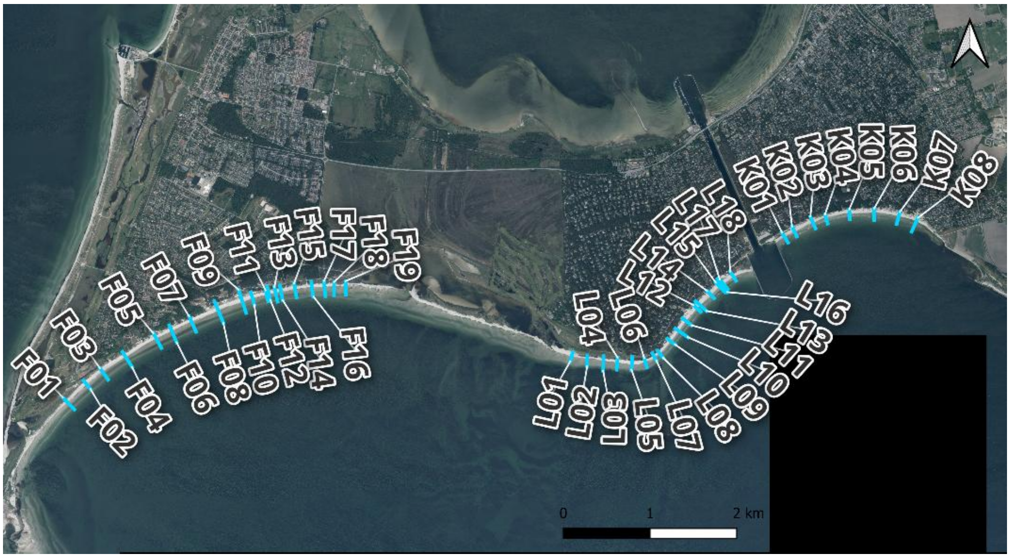

Figure 3.3: Map illustrating the 36 cross-shore transects used for topographical measurements and sediment sampling. The transects are categorized by beach: Falsterbo (F01-F19), Ljunghusen (L01-L18), and Kämpinge (K01-K08). (Orthophoto data source: Lantmäteriet)

3.2 Storm Babet

In October 2023, storm Babet caused severe erosion along the Swedish South coast. Sustained winds from southwest prior to the event pushed approximately 20 km^3 of water into the Baltic Sea through the Öresund strait (Bokhari Irminger et al., 2024). On October 18, the wind direction changed rapidly from west to east and increased in speed. This shift in wind direction, combined with the large volume of water already present in the semi-enclosed Baltic basin, resulted in significant elevated sea levels (Bokhari Irminger et al., 2024).

Across the region in Scania studied by (Bokhari Irminger et al., 2024), the estimated total sediment erosion was nearly 1.3 million cubic meters. The impact also extended to damage to structures such as roads, residential buildings and harbors. When comparing Babet to previous storm events, the recorded sea levels were high but not unprecedented. For example, during a storm in January 2017, a weather station in Skanör recorded a maximum sea level of 154 cm above mean sea level, which is higher than the 135 cm recorded during storm Babet. Despite the higher water level during the 2017 event, the coastal damage was more severe during Babet. This difference is explained by the wave conditions. Babet presented a combination of high sea levels and significant wave heights considerably higher than during the 2017 event (Bokhari Irminger et al., 2024).

The erosive impact of storm Babet resulted in the formation of distinct dune scarps, illustrated in Figures 3.4 and 3.5. These photographs were taken the day after the storm at Falsterbo and Ljunghusen beaches, respectively.

Figure 3.4: Dune scarps at Ljunghusen beach the day after the storm in October 2023. (Photo: Caroline Hallin)

Figure 3.5: Dune scarps at Falsterbo beach the day after the storm in October 2023. (Photo: Caroline Hallin)

3.3 Data

This study uses data provided by external sources and previous research. The historical orthophotos used are presented in Table 3.1. The topographic measurements shown in table 3.2 are taken in the same cross shore transects that are used in this study and serve as a necessary baseline to compare with the field data collected in this thesis.

Table 3.1: Orthophotos used in the vegetation line and beach width analysis.

Data source	type	pixel size (m)	year
Lantmäteriet	Orthophoto	0.16	2024
Vellinge kommun	Orthophoto	0.16	2022
Vellinge kommun	Orthophoto	0.16	2020
Lantmäteriet	Orthophoto	0.25	2018
Vellinge kommun	Orthophoto	0.08	2017
Lantmäteriet	Orthophoto	0.25	2016
Lantmäteriet	Orthophoto	0.25	2014
Lantmäteriet	Orthophoto	0.25	2012
Lantmäteriet	Orthophoto	0.25	2009
Lantmäteriet	Orthophoto	0.5	2007
Lantmäteriet	Orthophoto	0.5	2004
Vellinge kommun	Orthophoto	1.0	1999
Vellinge kommun	Orthophoto	0.5	1973
Lantmäteriet	Orthophoto	0.5	1960
Lantmäteriet	Orthophoto	1.0	1939

Table 3.2: Topography measurements used in dune volume calculations

Measured by	Type	date
Emmy Sukchaiwan	Topography (GNSS)	2023-03-28
Emmy Sukchaiwan	Topography (GNSS)	2023-10-24
LTH	Topography (GNSS)	2023-10-22
LTH	Topography (GNSS)	2024-09-30
LTH	Topography (GNSS)	2025-01-28
LTH	Topography (GNSS)	2025-04-22
LTH	Topography (GNSS)	2025-10-14

4 Methodology

The methodology is structured around three primary analytical components: spatial and temporal analysis of the vegetation line and beach width using GIS, spatial grain size distribution through sediment sampling and sieving, and analysis of dune morphology changes over time.

4.1 Vegetation line and beach width analysis in GIS

To analyze the spatial variations of the vegetation line over time, orthophotos provided by Lantmäteriet and Vellinge municipality were utilized. In total, orthophotos from 14 different years between 1939 and 2024 were used.

The vegetation line was digitized by manually tracing the border between the bare beach and vegetation using the “Add Line Feature” tool in QGIS. To maintain consistency and minimize bias, all vegetation line digitization were created at a fixed zoom level of 1:200. Intersection points were then generated where the vegetation line crossed the predefined cross shore transects. The distance from these points to a fixed baseline was calculated for all corresponding years. To get results for the vegetation line movement for a stretch of a beach, two or three transect were grouped together and the average measured distance from the base line was then calculated.

To clearly visualize the historical migration of the vegetation line, the distance measured in the earliest available year was subtracted from all subsequent years. This approach normalizes the initial measurement to 0 meters and allows the relative progradation or landward retreat of the vegetation line to be presented as distance from the starting point for each year.

The shoreline was digitized by tracing the boundary between the beach and the water, following the same methodology used for the vegetation line. The beach width for each year was then calculated as the cross shore distance between the shoreline and the vegetation line at each specific transect. The average beach width per year for each beach was also calculated.

4.2 Sediment samples and sieving

To analyze spatial variations of sediment along the southern Falsterbo coastline a field sampling campaign in March 2026 was carried out across 34 cross shore transects along the beaches of Falsterbo, Ljunghusen and Kämpinge. Four samples were collected at each transect.

To capture the cross shore variability within each transect, sediment samples were collected at four specific morphological zones: The swash zone, mid-beach, dune toe and dune crest as illustrated in figure 2.1.

The sampling method was designed to exclusively target the uppermost active sediment layer which is most susceptible to aeolian transport. This was achieved by carefully scraping the top layer to a depth of 5-10 mm using a flat metal scraper. A sediment volume of 100 ml was collected and sealed in labeled plastic bags at each measurement point to ensure consistency across all 136 samples.

The samples were washed in tap water to remove soluble salt and organic debris before being oven dried at 105˚C for 12 hours to remove moisture. Each sample where sieved in a Retsch Sieve shaker AS 200 basic for 15 minutes in a stack consisting of the following mesh sizes: 2, 1.4, 1, 0.71, 0.5, 0.355, 0.25, 0.18, 0.125, 0.09, 0.063 mm along with the bottom pan. The sediment fraction collected on each sieve was individually weighed on a scale with a precision of 0.1g and documented for each sample. The resulting data was processed in a python script that calculates the cumulative passing percentage by mass for each sample and uses linear interpolation to determine the grain sizes. The resulting parameters represent the grain diameters where 50% (the median, D50), 16% (D16), and 84% (D84) of the sorted sediment sample is finer by mass.

4.3 Topographic Surveys

Cross shore topographic profiles were measured using a Global Navigation Satellite System (GNSS) rover (NcGeo-S4I). The topographic surveys were conducted along 36 transects in the study area. The acquired GNSS data were integrated with existing historical transect data, including profiles captured immediately before and after the storm Babet in October 2023 (Sukchaiwan, 2023). For each transect a python script was used to calculate the change in cross-sectional dune volume expressed in (m^3/m) of alongshore width between two measurement dates in the same transect. Specifically, the script calculates the cross sectional area changes between the profile curves through integration using the trapezoidal method.

In some cases, the GNSS measurements from earlier dates did not capture the entire active dune stretch needed to calculate the volume change accurately. To address this data limitation, measurements from another date that is sufficiently close in time were used to join and extend the measured transect. The resulting cross shore profile were visually controlled to not include clear "jumps" in the splice of the two profiles.

To calculate the recovery of dune sediment volume, the topography measurements taken the days after the storm (October 2023) are compared against the measurements taken in March 2026. Measurements from 2023-03-28 (pre storm) are compared to measurements taken in the days after the storm to calculate erosion volume.

Since this study focuses specifically on the dune as a part of the beach sediment system, it was necessary to there isolate the volumetric changes of the dunes from the rest of the beach. To achieve this, cross shore boundaries were manually defined for each transect after analyzing the topographical profiles. The landward limit was set at the point where the GNSS measurements converged, indicating no meaningful morphological change. The seaward boundary was defined by the location of the dune toe. Manually setting this seaward limit was important, as localized piles of seaweed (wrack) mixed with sand were present on the lower beach during the time of measurement. By placing the boundary at the dune toe, these temporary deposits were excluded, ensuring that the calculated volumes accurately represent actual aeolian dune recovery.

To visualize the transect profile and the areas that are calculated, a plot for each transect was made. In Figure 4.1 and 4.2, an example (F07) of what these profile plots look like are shown. Areas in green represent accumulated volumes and areas in red represent eroded volumes. The computed accretion and erosion volumes across all transects were then compiled into bar charts.

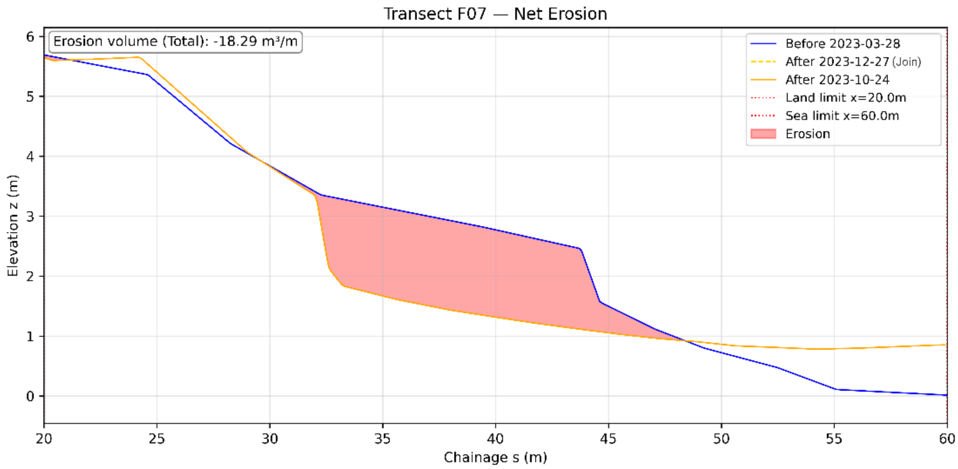

Figure 4.1: Cross-shore topographic profile for transect F07 comparing before and after storm measurements. The red shaded area indicates the sediment volume (m^3/m) eroded during Storm Babet.

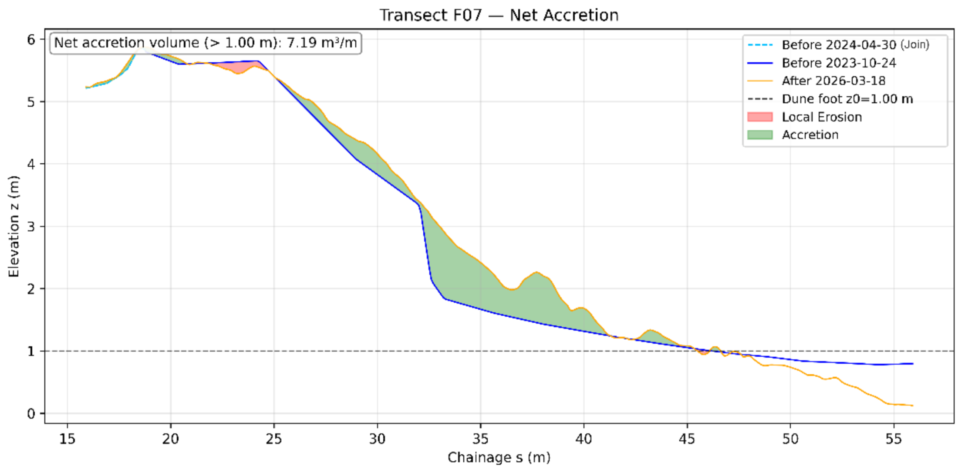

Figure 4.2: Cross-shore topographic profile for transect F07 demonstrating post-storm dune recovery. The green shaded area indicates the sediment volume (m^3/m) aeolian accumulation between October 2023 and March 2026.

The topography dataset before the storm Babet was limited to seven transects on Falsterbo Beach and two on Ljunghusen Beach. Consequently, storm erosion volumes could only be calculated for these nine profiles, whereas post storm recovery volumes could be calculated across all 36 transects

4.4 Correlation analysis

To investigate the underlying factors causing spatial variations in the post storm dune recovery of the study area, a correlation analysis was conducted. A

Python script was used to generate scatterplots comparing a specific data parameter of each transect against its net sediment accumulation volume measured between October 2023 and March 2026. To evaluate the strength and significance of these correlations, the Spearman rank correlation coefficient (ρ) was calculated for each parameter pair according to equation 1:

$$\rho = 1 - \frac{6\sum_{i=1}^{n} d_i^2}{n(n^2-1)} \qquad (1)$$

Where d_i is the difference between the ranks of corresponding values for a given transect, and n is the total number of evaluated transects.

The Spearman coefficient evaluates the direction and strength of the monotonic relationship between the variables, while the associated p-value (p) is used to determine statistical significance of this correlation. A threshold of $p < 0.05$ is defined as statistically significant, this means that if there were no actual correlation, the chance of seeing these results is less than 5%. Results falling within $0.05 < p < 0.1$ are considered marginally significant and conclusions drawn from results values in this range should be analyzed with caution. The coefficient of determination (R^2) was calculated and indicates how well the data points fit the trendline.

5 Results

5.1 Dune Volume and Morphological Changes

The erosion data presented in figure 5.1 shows that all transects with available pre-storm measurements experienced a volumetric loss exceeding 10 m^3/m of dune sand. Since pre-storm measurements were only available for nine transects, it is difficult to make a comprehensive comparison of the storm impact across the whole peninsula. However, the result indicates that most transects have only recovered a fraction of the volume eroded by the storm. For the nine transects where pre-storm data is available, the average volumetric recovery is 53%. Transect F05 had the least percentual recovery (12%) and F09 the highest (138%).

Figure 5.1: Dune erosion (red) from Storm Babet and the subsequent net accretion (green) measured between October 2023 and March 2026.

During the recovery period between October 2023 and March 2026, the aeolian sand transport showed large spatial differences. Presented in figure 5.2, a trend from west to east can be seen in the net accretion for all 36 transects. The Falsterbo (F) transects in the west generally show the highest recovery volumes. Transect F09 had the highest recovery with a net accretion of 17.6 m^3/m, and it is the only measured transect that has fully recovered to its pre-storm volume. Moving east, the Ljunghusen (L) transects show moderate recovery, while the Kämpinge (K) transects in the east show the lowest recovery, with several transects close to 0 m^3/m. Despite these localized peaks in accumulation, the overall trend indicates that most transects have only recovered a small fraction of their pre-storm volume.

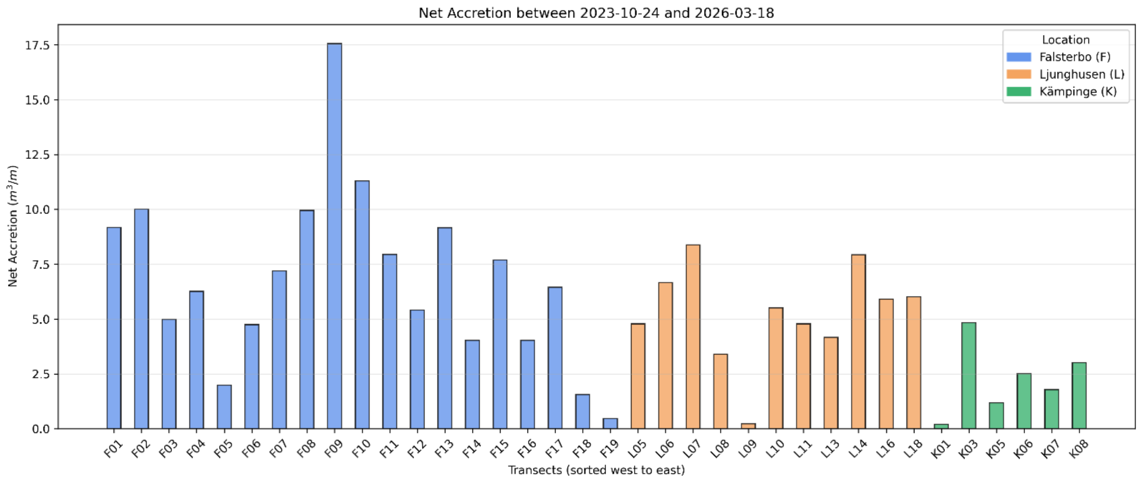

Figure 5.2: Net aeolian dune accretion (m3/m) across all 36 transects from October 2023 to March 2026, sorted west to east.

Analyzing specific cross shore profiles, such as transect F07 (Figure 4.2), reveals how the dunes rebuild structurally. The high water levels during Storm Babet eroded the dune toe and created a steep dune scarp. The post-storm data shows that the Aeolian transported sand is deposited directly against this steep eroded face and thereby recovers the dune, shown by the green accretion area. However, because the total recovery volumes are still low compared to the erosion, the dunes remain vulnerable to future storm events.

5.2 Beach width and Vegetation Line

Across all analyzed coastal sections, a distinct and sudden landward retreat of the vegetation line is visible between the measurements from 2022 and 2024. This acute retreat is a direct result of Storm Babet in October 2023, where the vegetation was removed when the dunes they grew on were eroded. While the majority of the stretches along the coastline show a long term trend of progradation since 1939, the vegetation line change in the years prior to the storm show important local variations.

Falsterbo Beach

There is a clear historical trend of progradation on the Falsterbo beach where the vegetation line steadily advanced towards the sea from 1939 until roughly 2012 (Figure 5.4). Around this time, the system appears to have reached an equilibrium or a turning point, where the general progradation stopped. Looking at the more recent relative changes between 2012 and 2024 (Figure 5.5), a clear spatial sorting along the beach becomes visible. The eastern sections (represented by the blue and green lines) have retreated significantly, while the westernmost section (purple line, F01-F03) has remained stable or even advanced. This dynamic indicates a "beach rotation", where the beach is eroding in the east, and the longshore sediment transport moves that material to accumulate in the west, thereby rotating the shoreline orientation. Figure 5.3 illustrates the location of the beach stretches measured and presented in figures 6.4 and 6.5.

Figure 5.3: Location of the beach stretches at Falsterbo beach where the vegetation line was compared (Orthophoto data source: Lantmäteriet).

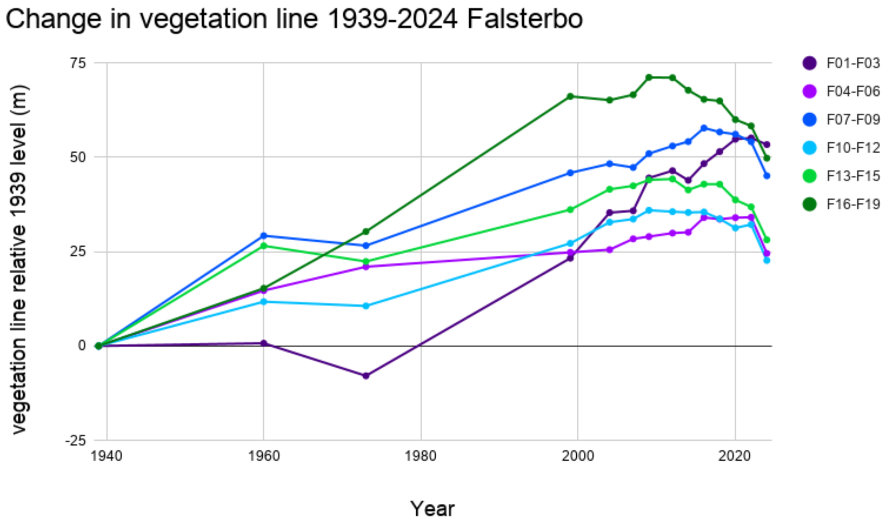

Figure 5.4: Changes in the vegetation line at Falsterbo beach relative to the 1939 level.

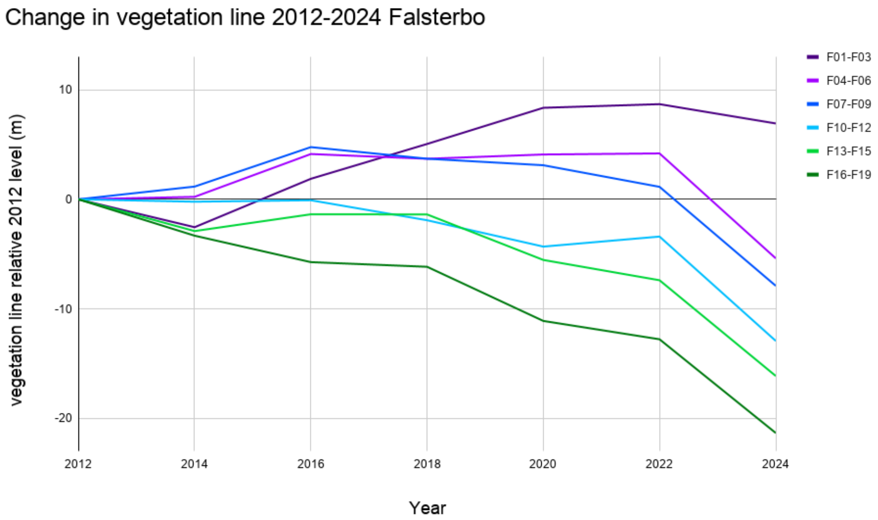

Figure 5.5: Changes in the vegetation line at Falsterbo beach relative to the 2012 level.

Ljunghusen Beach

The Ljunghusen beach shows a higher spatial variation across both time periods (Figures 5.7 and 5.8). Historically, the westernmost section and the protruding headland in the middle of the beach have retreated landward since 1939 (Figure 5.7). Headlands naturally attract more wave energy due to wave refraction, making them more vulnerable to erosion. In contrast, the two easternmost sections have experienced massive progradation, which is a consequence of the construction of the Falsterbo Canal in 1940. The breakwaters of the canal act as barriers that interrupt the longshore sediment transport and forcing sand to accumulate on the beach adjacent to the structure. However, In the recent decade from 2012 to 2024 (Figure 5.8), the entire beach stretch shows a trend of erosion with the central sections experiencing the largest vegetation line retreat leading up to and including Storm Babet.

Figure 5.6: Location of the beach stretches at Ljunghusen beach where the vegetation line was compared (Orthophoto data source: Lantmäteriet).

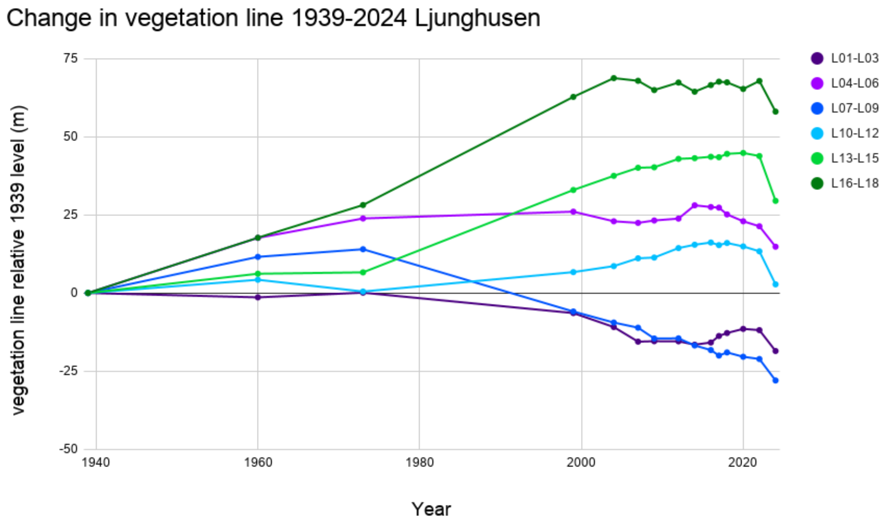

Figure 5.7: Changes in the vegetation line at Ljunghusen beach relative to the 1939 level.

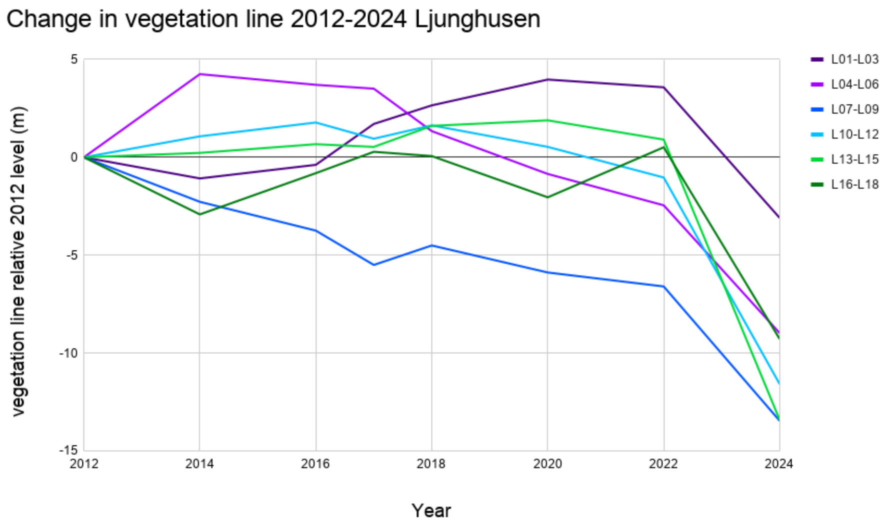

Figure 5.8: Changes in the vegetation line at Ljunghusen beach relative to the 2012 level.

Kämpinge Beach

The Kämpinge beach have a consistent historical progradation across all analyzed sections since 1939 (Figure 5.11). Like Ljunghusen, the section closest to the canal structure has grown the most. This further confirms the impact of the Falsterbo canal trapping sediment along the coast. In the more recent period between 2012 and 2024 (Figure 5.10), the Kämpinge beach appears to be the most stable of the three studied areas. Apart from the distinct retreat caused by Storm Babet at the end of the time series, there is no significant background trend, and the different sections of the beach behave relatively uniformly without signs of rotation.

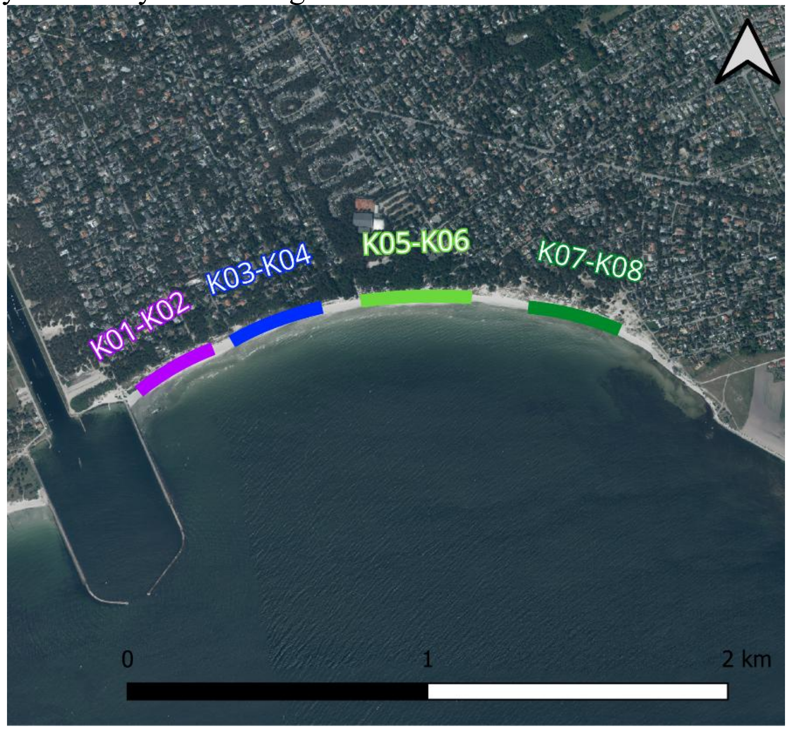

Figure 5.9: Location of the beach stretches at Ljunghusen beach where the vegetation line was compared (Orthophoto data source: Lantmäteriet).

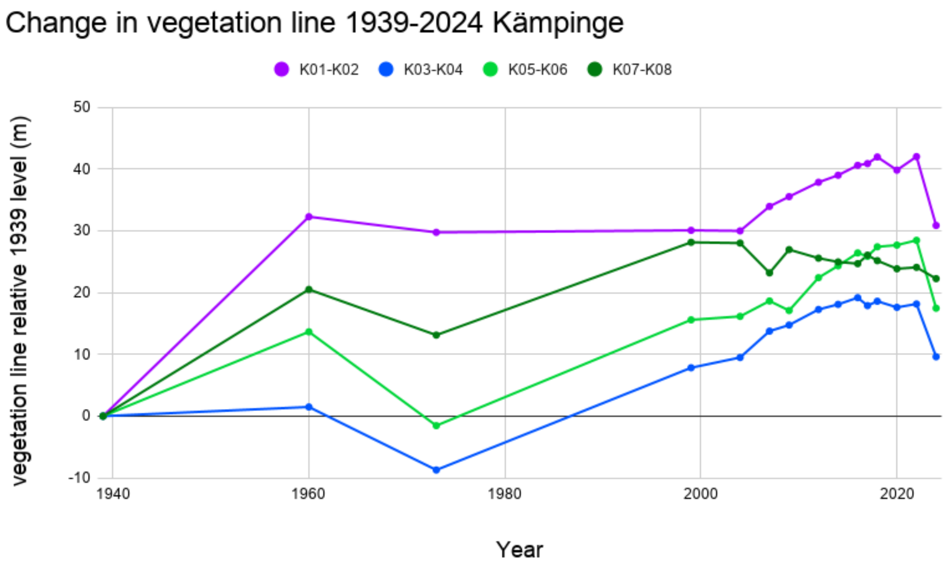

Figure 5.10: Changes in the vegetation line at Kämpinge beach relative to the 1939 level.

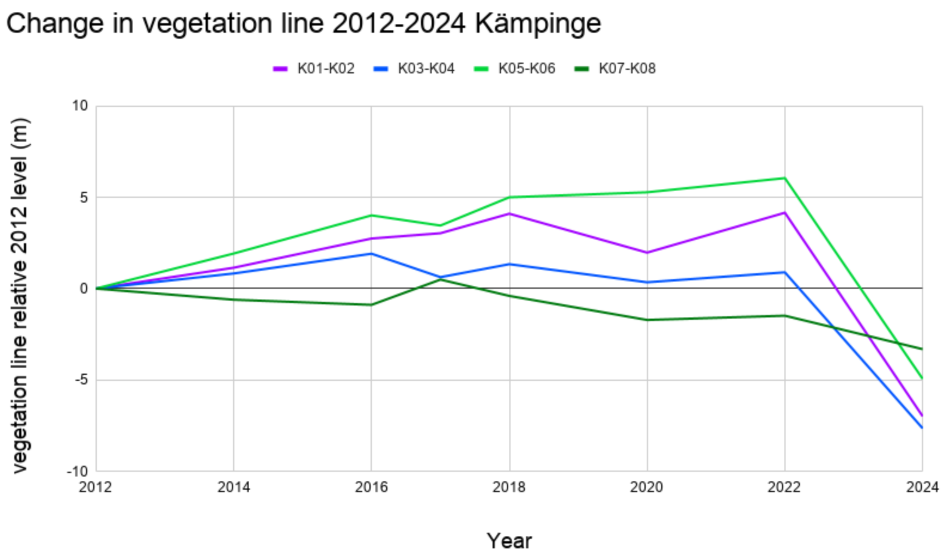

Figure 5.11: Changes in the vegetation line at Kämpinge beach relative to the 2012 level.

An important limitation in the long term analysis is the uneven spread of data points over time. The density of data is significantly higher from 1999 to 2024 compared to the earlier years between 1939 and 1999. Most notably there is gap in data between 1973 and 1999 where no orthophotos were available. The gap creates uncertainty and acts as a potential source of error and might hide a much more active and changing beach with periods of erosion and recovery than the figures currently show.

Beach Width

Analyzing the beach width over time provides perspective on the area between the shoreline and the dune toe. A consistent observation across all three locations is the substantial increase in beach width recorded after Storm Babet in 2023. The eroding effect of the storm moves the dune toe and the vegetation line landward and the distance between the shoreline and dune toe therefore increases, resulting in a wider beach. Upon reviewing the results, each transect showed little variation in increase and decrease in relation to each other when viewed in a in a line diagram, The average beach width is therefore presented in figures 5.12, 5.13 and 5.14, but the specific data for each transects beach width is further analyzed in section 5.4 Correlation analysis. Beach width for each transect is shown in figure A.18, A.19 and A.20 in the appendix.

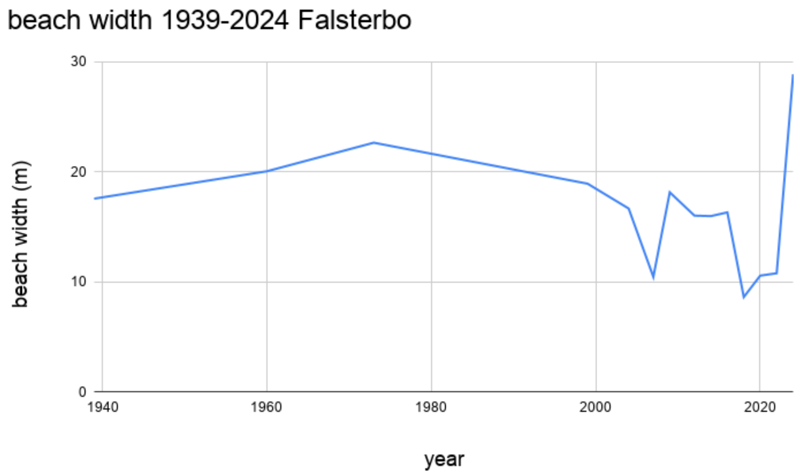

Figure 5.12: average beach width (m) at Falsterbo beach from 1939 to 2024.

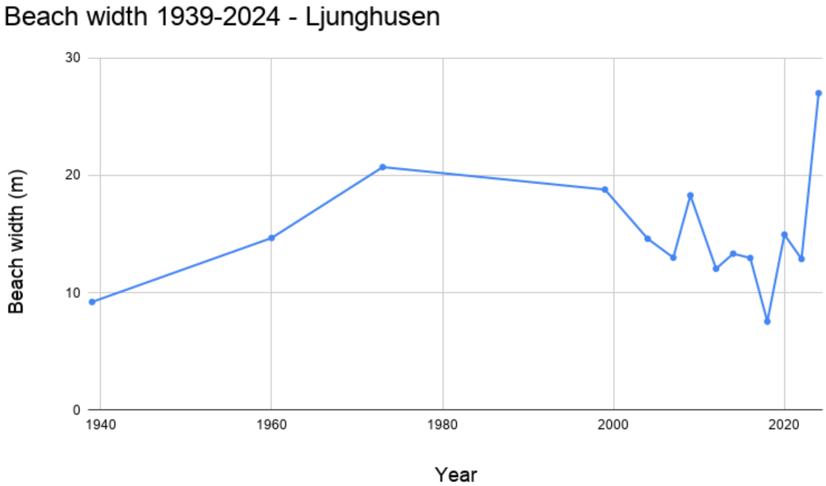

Figure 5.13: average beach width (m) at Ljunghusen beach from 1939 to 2024.

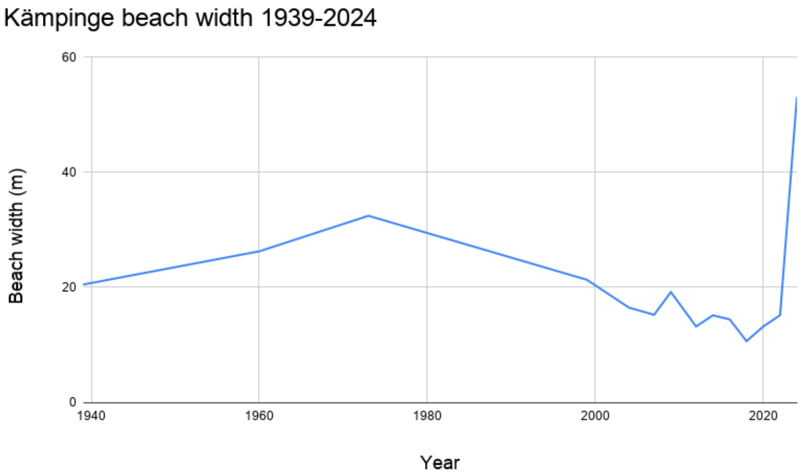

Figure 5.14: average beach width (m) at Kämpinge beach from 1939 to 2024.

5.3 Spatial Grain Size Distribution

The grain size distribution analysis based on the D50 parameter shows a generally homogenous sediment composition along the southern coast of the Falsterbo peninsula, with no prominent longshore trend from west to east. Cross shore analysis between the four morphological zones: the swash zone (A), mid-beach (B), dune toe (C), and dune crest (D) (seen in figure 5.15) shows marginal variations. Across the majority of the transects, the D50 values for the aeolian-dominated zones (C and D) are similar to the wave-dominated zones (A and B), meaning the sediment at the dune crest is not significantly finer than the sediment found anywhere else on the beach (Figure 5.16, 5.17, 5.18).

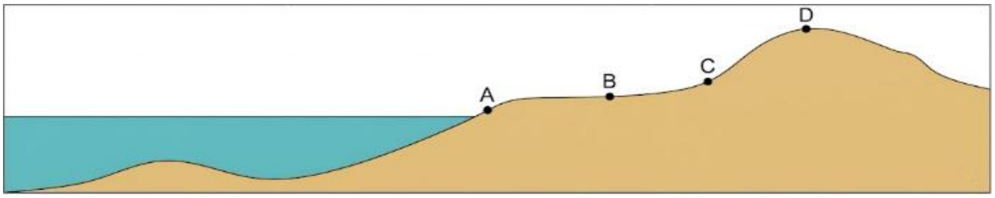

Figure 5.15: A general cross shore profile with the four morphological zones (A: swash zone, B: mid-beach, C: dune toe, D: dune crest). (Figure modified from (Hallin et al., 2019) by Google gemini).

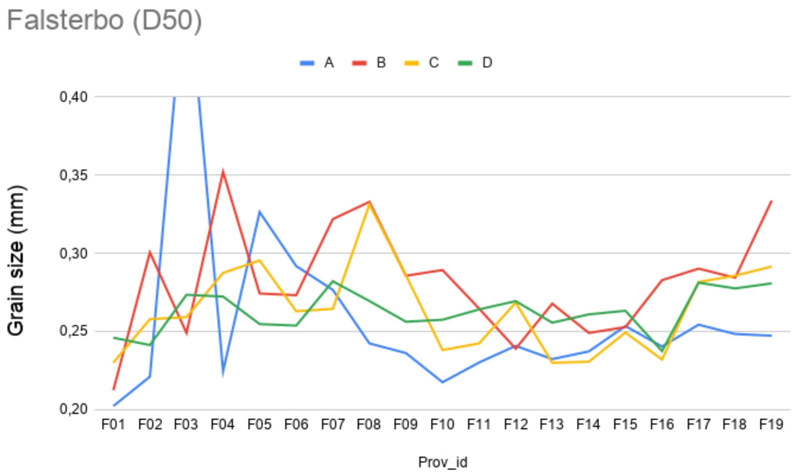

Figure 5.16: Median grain size (D50) across the Falsterbo beach (sorted west to east) for the four morphological zones shown in figure 5.15.

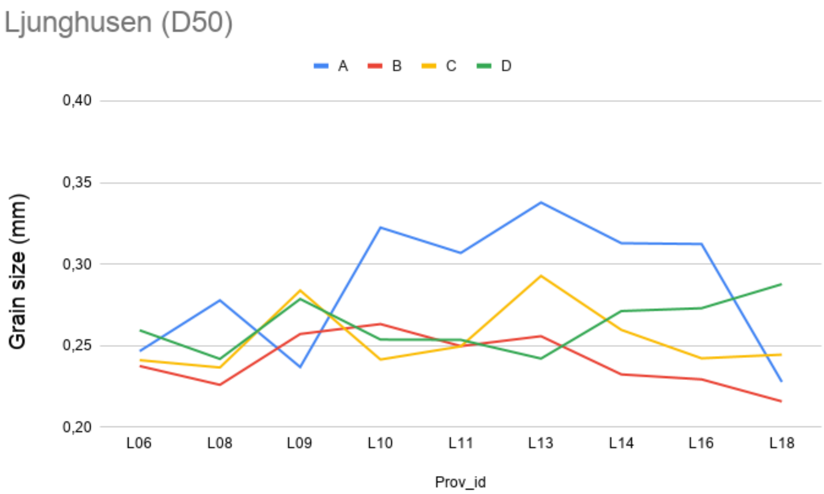

Figure 5.17: Median grain size (D50) across the Ljunghusen beach (sorted west to east) for the four morphological zones.

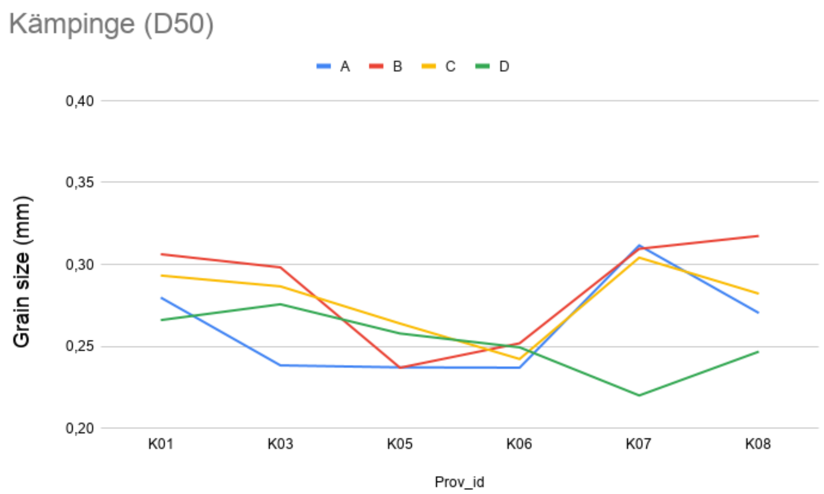

Figure 5.18: median grain size (D50) across the Kämpinge beach (sorted west to east) for the four morphological zones.

The absence of a cross shore sorting gradient indicates that the aeolian transport processes along the peninsula have in recent time transported the entire available grain size spectrum, and could be explained by wind velocities that regularly exceed the threshold velocities of the coarsest fractions present in the study area (Shao, 2009). This homogeneity could be due to the beach source material present at the Falsterbo peninsula is inherently well sorted and lacks a distinct coarse fraction. Additionally, the lack of a longshore grain size trend indicates a dynamic system where changing wave and wind directions is continuously mixing the sediment, preventing longshore sorting over the studied areas. The sediment sample sorting (D84, D16) can be seen in figure A.21, A.22 and A.23 in the appendix.

5.4 Correlation analysis

The resulting values for each scatter correlation are presented in Table 5.1, with the most significant p-values highlighted in bold. The analysis reveals a general lack of strong correlation across the majority of the measured variables. When comparing the pre-storm vegetation line migration rates and beach width (2024) with accumulated sediment volume, many of the datasets have p-values approaching 1.0, indicating a random distribution of points without any trend. However, The Falsterbo beach stands out, with marginally significant to significant trends in Beach width, Vegetation line change and swash zone grain size (D50).

Although the correlation between beach width (in 2024) and net accretion in Falsterbo is only marginally significant ($\rho = 0.43$, $p = 0.066$), it could suggest a trend where wider beaches in Falsterbo lead to higher dune accumulation rates. This is likely explained by a larger fetch area for aeolian transport. This relationship is entirely absent in the Ljunghusen and Kämpinge sections, where the data points appear random ($p = 0.555$ and $p = 0.704$ respectively). Similarly, the change in the vegetation line between 2012 and 2022 show a weak positive trend with accretion only on the Falsterbo beach ($\rho = 0.43$, $p = 0.064$), where Kämpinge and Ljunghusen beaches showed no statistical significance in correlation.

The measured parameter with most prominent statistical correlation against dune accumulation in the study was the median grain size (D50) in the swash zone (Part A). As detailed in Table 5.1, there is a statistically significant negative correlation for the Falsterbo beach ($\rho = -0.58$, $p = 0.013$), as well as the entire study area combined ($\rho = -0.39$, $p = 0.024$). This negative correlation indicates that finer sand grains present in the swash zone correlate with higher rates of aeolian dune growth and recovery.

Median grain size (D50) in the dune toe for the whole study area, displayed a negative correlation with marginal significance ($\rho = -0.33$, $p = 0.056$). In contrast, sediment sampled from the mid-beach (Part B), and dune crest (Part

D) showed no significant correlation with accretion volumes across any of the studied coastal stretches. The scatterplots with the lowest recorded p-values, which represent the strongest observable correlations, are presented in Figures 5.19 to 5.24. All remaining scatterplots are presented in the appendix.

Figure 5.19 illustrates the relationship between the volume of sediment eroded during Storm Babet and the subsequent net accretion. The statistical analysis yields no significant correlation ($\rho = -0.02$, $p = 0.966$). This suggests that the volume of erosion a specific dune section experiences does not dictate the rate of natural recovery. One could expect both a positive and negative correlation here. High erosion volume could be a sign that this part of the shoreline is chronically eroding and retreating inland. On the other hand, high dune erosion could lead to a wider beach and more sediment availability for the cross shore transport direction therefore leading to a faster recovery rate.

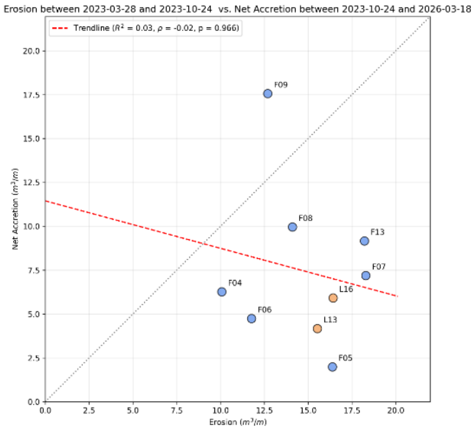

Figure 5.19: Scatter plot illustrating the correlation between the sediment volume eroded during Storm Babet and the subsequent net dune accretion.

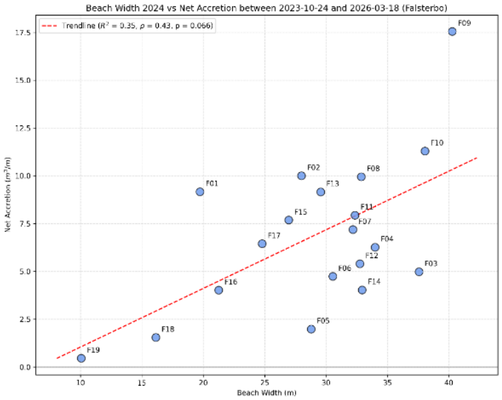

Figure 5.20 Scatter plot illustrating the correlation between measured beach width in 2024 and net dune accretion for the Falsterbo beach transects

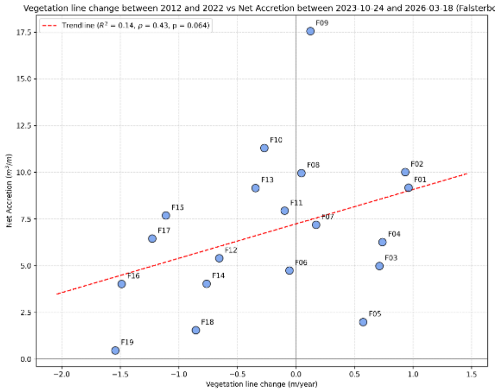

Figure 5.21: Scatter plot illustrating the correlation between the pre storm vegetation line migration rate (2012–2022) and net dune accretion at Falsterbo transects.

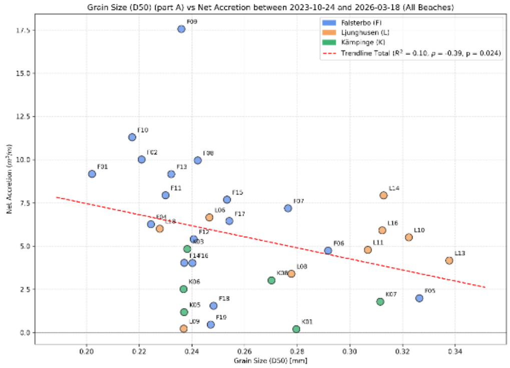

Figure 5.22: Scatter plot illustrating the correlation between median grain size (D50) in the swash zone (A) and net dune accretion for the whole study area.

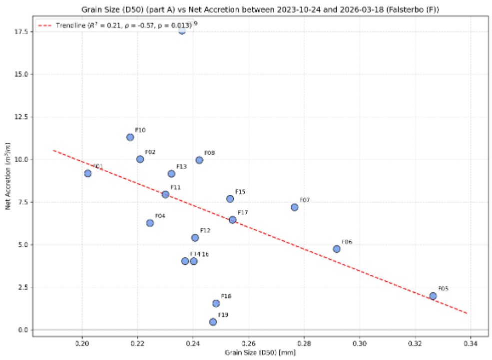

Figure 5.23: Scatter plot illustrating the correlation between median grain size (D50) in the swash zone (part A) and net dune accretion for Falsterbo transects.

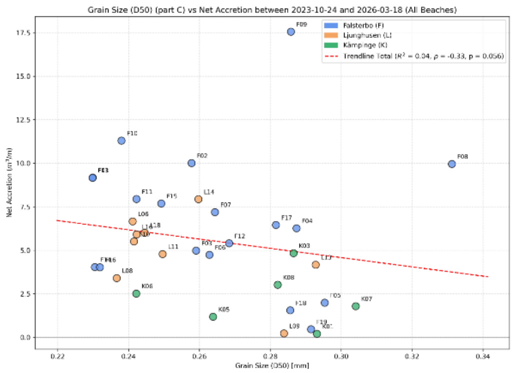

Figure 5.24: Scatter plot showing the correlation between the median grain size (D50) at the dune toe (part C) and net dune accretion across all analyzed transects.

Table 5.1: Spearman rank correlation coefficients (ρ) and corresponding p-values evaluating the relationship between parameters (erosion, vegetation line change, beach width, and median grain size D50) and net aeolian dune accumulation (m^3/m) measured between October 2023 and March 2026. Values marked with an asterisk (*) indicate statistically significant ($p < 0.05$) or marginally significant ($0.05 < p < 0.1$) correlations.

Correlation analysis	**Beach**	**Part**	R^2	**Spearman (ρ)**	**P - value**
Erosion	All	-	0.03	-0.03	0.966
Vegetation line change 2012-2022	Falsterbo	-	0.14	0.43	**0.0638***
Vegetation line change 2012-2022	Ljunghusen	-	0.01	-0.02	0.958
Vegetation line change 2012-2022	Kämpinge	-	0.12	-0.54	0.266
Vegetation line change 2012-2022	All	-	0.01	-0.03	0.843
Beach width 2024	Falsterbo	-	0.35	0.43	**0.0663***
Beach width 2024	Ljunghusen	-	0.00	-0.20	0.555
Beach width 2024	Kämpinge	-	0.10	-0.20	0.704
Beach width 2024	All	-	0.01	-0.13	0.468
Grain size (D50)	Falsterbo	A	0.21	-0.58	**0.0126***
Grain size (D50)	Ljunghusen	A	0.07	0.03	0.932
Grain size (D50)	Kämpinge	A	0.15	-0.26	0.623
Grain size (D50)	All	A	0.10	-0.39	**0.0242***
Grain size (D50)	Falsterbo	B	0.00	0.07	0.775
Grain size (D50)	Ljunghusen	B	0.18	-0.37	0.332
Grain size (D50)	Kämpinge	B	0.03	0.20	0.704
Grain size (D50)	All	B	0.00	-0.03	0.852
Grain size (D50)	Falsterbo	C	0.01	-0.24	0.327
Grain size (D50)	Ljunghusen	C	0.24	-0.18	0.637
Grain size (D50)	Kämpinge	C	0.01	-0.20	0.704
Grain size (D50)	All	C	0.04	-0.33	**0.0563***
Grain size (D50)	Falsterbo	D	0.09	-0.24	0.325
Grain size (D50)	Ljunghusen	D	0.01	0.37	0.332
Grain size (D50)	Kämpinge	D	0.06	0.03	0.957
Grain size (D50)	All	D	0.00	0.03	0.850

6 Discussion

The observed lack of cross shore grain size sorting contradicts typical aeolian transport models, such as those described by (Hoonhout and Vries, 2016) and (Bagnold, 1941) which anticipate that larger grain sizes remain on the mid-beach and finer sediment are transported downwind and deposited on the dune surface. The homogeneity observed across the southern Falsterbo peninsula could mean that the local sediment supply may be inherently well sorted with no distinct coarse fraction to be left behind on the mid-beach. Second, the dynamic wind and wave climate of the peninsula might be continuously mixing the surface layer, preventing a stable longshore sorting gradient over time.

Studies of post storm recovery on similar coastal dune systems by Burvingt and Castelle (2023), indicate that full dune recovery usually takes multiple years, given that the system is not interrupted by further storm events. This is consistent with this theisis results average dune volume recovery of 53% after three years The large spatial variability in recovery, where Falsterbo recovered significantly better than Kämpinge, cannot be explained by grain size alone. The marginally significant correlation between beach width and accretion at Falsterbo ($\rho = 0.43$) might suggest that the fetch length is a limiting factor. However, the actual fetch length depends on wind direction relative to the shoreline. Winds blowing at an angle or parallel to the beach increase the distance the wind travels over dry sand. This factor has not been studied in this thesis but could explain a part of the variations in dune growth.

6.1 Implications for Coastal Management

The historical analysis of the vegetation line indicates that the long-term progradation of the Falsterbo shoreline shifted around 2012, transitioning into a state of equilibrium or retreat. Together with the finding that aeolian transport has only recovered an average of 53% of the eroded dune volume across the measured transects, implies that the dunes remain highly vulnerable to consecutive extreme weather events and the shoreline might face further retreat in the future.

For coastal management in this area, this implies that relying only on natural aeolian recovery for flood protecting dunes may be insufficient, particularly for the Ljunghusen and Kämpinge beaches where dune growth is lowest. Sand nourishment may be necessary to maintain the dunes protective capacity. The median grain size of the nourishment might also play a role, as this study indicates that finer sand in the swash zone and dune toe could lead to greater dune recovery.

Finally, the municipality does not currently monitor dune volumes. Without monitoring, there is no way to know if the dunes have eroded past critical safety levels. Given that the constructed dikes and walls along the peninsula are designed to withstand sea levels up to +3.0 m (RH2000), an investigation to determine the dimensioning dune volume required to provide an equivalent level of protection is recommended. Without establishing and maintaining the critical volumes, the sand dunes risk becoming the weak link in the peninsulas flood defense infrastructure. Introducing a monitoring program could alert coastal managers when a part of the dune system has eroded beyond the critical volume. The beach rotation observed at Falsterbo beach in this thesis (Section 5.2) likely represents a system striving towards equilibrium dictated by the wind and wave climate. The investigation should therefore include a one-line shoreline model to predict future shoreline changes.

6.2 Uncertainty and future research

The results in this study are subject to methodological uncertainties. A primary limitation is the availability of the pre-storm GNSS data, which was limited to only nine transects. Consequently, the calculation of storm erosion and the resulting recovery for the whole study area is based on this limited data. The historical vegetation line analysis contains a data gap between 1973 and 1999 due to the unavailability of orthophotos. This 26-year absence introduces uncertainty, as it might hide prominent trends that could challenge the assumption that most shoreline stretches have been prograding steadily from 1939 to 2012. Further limitation of this method is the grouped transects where the vegetation line was measured. Because the transects are not evenly distributed throughout the study area, the groups of transects represent different lengths along the beach, but all groups are represented equally as single lines in the presented charts. The resolution of the different orthophotos differ from 0.08 to 1.0 m pixel sizes and introduce a difference in uncertainty between different vegetation lines. This uncertainty is not presented or taken into consideration in the resulting charts.

Sediment sample F03-A deviates from the rest of the samples with significantly higher median grain size. The result was identified as an outlier and excluded from the correlation analysis to avoid skewing the results. This outlier creates uncertainty by suggesting a possibility of underlying sampling or processing errors affecting other samples.

The lack of strong statistical significance across several morphological and temporal variables proves that post storm dune recovery is a complex process that is not fully captured in this study. Future research in the area to better explain the variance in aeolian accumulation could include wind speed and wind direction relative to shoreline orientation, wave direction and bathymetry as well as the specific type and abundance of dune vegetation. Furthermore, the impact of human activity and beach users on sediment compaction and vegetation disruption could be quantified as it may significantly alter the natural recovery rates in populated areas like Falsterbo and Kämpinge.

7 Conclusion

The objective of this thesis was to analyze the post storm recovery of the sand dunes along the Falsterbo peninsula following the storm Babet in October 2023 and investigate the underlying factors driving spatial variations. Based on the research questions, the following conclusions are drawn:

- Extent of dune volume recovery: Natural recovery in the study area showed an average of 53% of the eroded dune volume returning by March 2026 across the measured transects. The recovery rates show significant spatial variation between the three studied beaches, Falsterbo beach in the west showed the highest accretion, while Kämpinge beach in the east showed the lowest and Ljunghusen somewhere in between. Some specific transects showed close to zero dune volume recovery
- Influence of beach characteristics:
    - **Vegetation line**: The vegetation line migration rate (2012-2022) showed marginally significant positive correlation with higher rates of dune accumulation only along Falsterbo beach ($\rho = 0.43$, $p = 0.064$). No significant correlation was found for Ljunghusen and Kämpinge beach.
    - **Grain size**: A statistically significant correlation was identified between finer median grain sizes (D50) in the swash zone and higher rates of net dune accumulation for Falsterbo beach and when combining all measured beaches. Additionally, a marginally significant negative correlation was observed at the dune toe (part C) across the entire study area combined ($\rho = -0.33$, $p = 0.056$). These results indicate that a

finer sediment supply in these zones generally supports higher rates of aeolian dune growth and recovery.

- **Beach width**: A marginally significant positive correlation was observed only at the Falsterbo beach ($\rho = 0.43$, $p = 0.066$), suggesting that a wider beach supports recovery by providing a larger fetch area for aeolian sediment transport. This relationship was statistically absent for Ljunghusen and Kämpinge beaches, indicating that beach width is a localized factor rather than a universal factor for the entire study area.

The long term progradation of the Falsterbo shoreline halted around 2012, vegetation line data indicates a long term progradation of the Falsterbo shoreline up until 2012, where the shoreline reaches its peak for the time period and in the latest decade has shifted towards an equilibrium state or coastal retreat. The significant retreat in vegetation line between 2022-2024 highlights the vulnerability of the dune system to storm events. The spatial distribution of dune recovery showed that Falsterbo in the west, exhibited the highest accretion, whereas Kämpinge in the east, showed the lowest accretion. While variables such as beach width and historical vegetation line migration showed only weak or localized correlations with recovery volume, sediment grain size proved to be a significant factor as statistically significant correlation was identified between the median grain size (D50) in the swash zone and net dune accumulation, indicating that the presence of finer sand might lead to higher rates of aeolian dune growth. Taking all of this into consideration, the dune system and in extension, the flood protection of the Falsterbo peninsula proves to be vulnerable to erosive storm events. This study proves that the natural recovery of the dunes proves to be slow and varies greatly, with one area only having 12% of the eroded volume returned three years after the storm. The dune areas that show less natural post storm recovery will likely need sand nourishment or other engineered solutions in order for the peninsula to maintain its flood protection.

8 References

Bagnold, R.A., 1941. The physics of blown sand and desert dunes. Methuen & Co, London.

Bokhari Irminger, S., Adell, Karlsson, M., Schöld, S., Magnusson, Å., 2024. Impact and response of storm Babet from a Swedish perspective 22 pages. https://doi.org/10.18171/1.094115

Burvingt, O., Castelle, B., 2023. Storm response and multi-annual recovery of eight coastal dunes spread along the Atlantic coast of Europe. Geomorphology 435, 108735. https://doi.org/10.1016/j.geomorph.2023.108735

Cohn, N., Ruggiero, P., De Vries, S., Kaminsky, G.M., 2018. New Insights on Coastal Foredune Growth: The Relative Contributions of Marine and Aeolian Processes. Geophysical Research Letters 45, 4965–4973. https://doi.org/10.1029/2018GL077836

Fredriksson, C., Larson, M., Hanson, H., 2017. LONG-TERM MODELLING OF AEOLIAN TRANSPORT AND BEACH-DUNE EVOLUTION. Coastal Dynamics.

Hallin, C., Almström, B., Larson, M., Hanson, H., 2019. THE RELATION BETWEEN LONGSHORE VARIATIONS IN GRAIN SIZE DISTRIBUTION AND SEDIMENT TRANSPORT PROCESSES, in: Coastal Sediments 2019. Presented at the International Conference on Coastal Sediments 2019, WORLD SCIENTIFIC, Tampa/St. Petersburg, Florida, USA, pp. 1269–1282. https://doi.org/10.1142/9789811204487_0111

Hoonhout, B.M., Vries, S.D., 2016. A process-based model for aeolian sediment transport and spatiotemporal varying sediment availability. JGR Earth Surface 121, 1555–1575. https://doi.org/10.1002/2015JF003692

Länsstyrelsen Skåne, 2021. Miljökonsekvensbeskrivning av riskhanteringsplan för Falsterbonäset (No. 2021:39). Länsstyrelsen Skåne, Malmö.

Michałowska, K., Głowienka, E., 2022. Multi-Temporal Analysis of Changes of the Southern Part of the Baltic Sea Coast Using Aerial Remote Sensing Data. Remote Sensing 14, 1212. https://doi.org/10.3390/rs14051212

Moore, L.J., Hacker, S.D., Breithaupt, J., De Vries, S., Miller, T., Ruggiero, P., Zinnert, J.C., 2025. Ecomorphodynamics of coastal foredune evolution. Nat Rev Earth Environ 6, 417–432. https://doi.org/10.1038/s43017-025-00672-z

Shao, Y. (Ed.), 2009. Physics and Modelling of Wind Erosion, Atmospheric and Oceanographic Sciences Library. Springer Netherlands, Dordrecht. https://doi.org/10.1007/978-1-4020-8895-7

Sukchaiwan, E., 2023. Dune Erosion on the Falsterbo Peninsula.

Vellinge kommun, 2025. Skyddsinvallning: Beskrivning av projektet i sin helhet.

9 Appendix

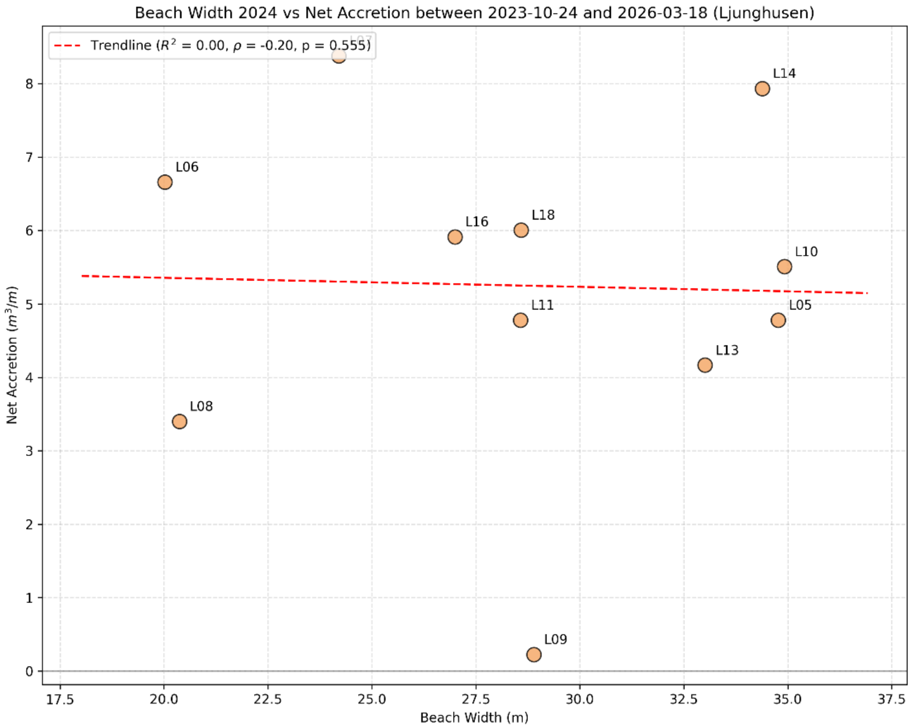

Figure A. 1: Scatter plot showing the correlation between measured beach width in 2024 and net dune accretion for Ljunghusen transects.

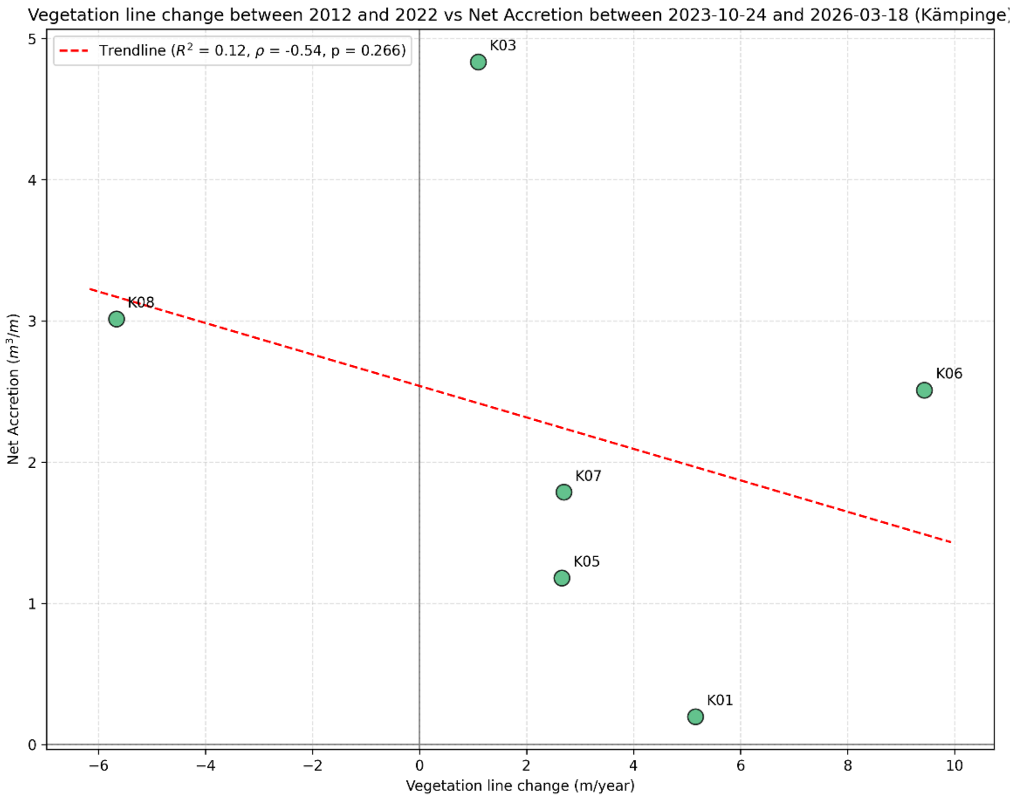

Figure A. 2: Scatter plot showing the correlation between the pre-storm vegetation line migration rate (2012–2022) and net dune accretion for Kämpinge transects.

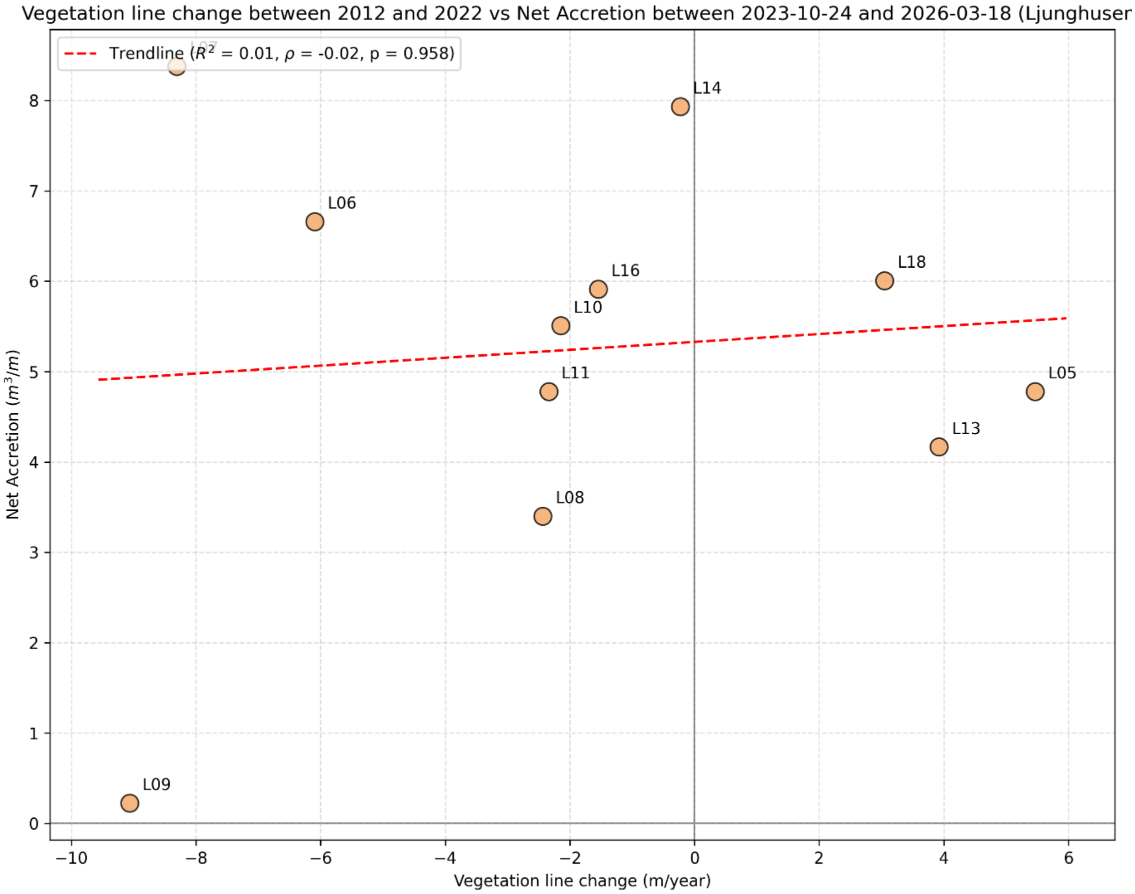

Figure A. 3: Scatter plot showing the correlation between the pre-storm vegetation line migration rate (2012–2022) and net dune accretion for Ljunghusen transects

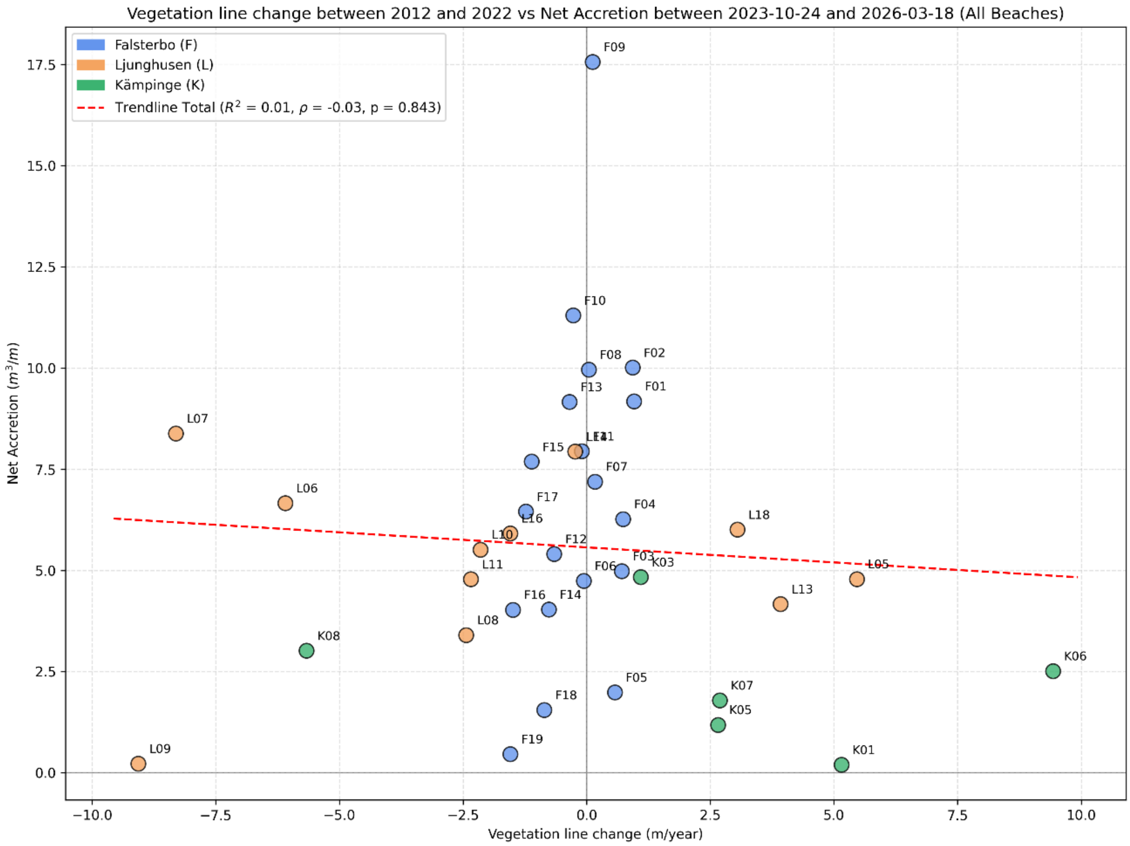

Figure A. 4 Scatter plot showing the correlation between the pre-storm vegetation line migration rate (2012–2022) and net dune accretion across all analyzed transects.

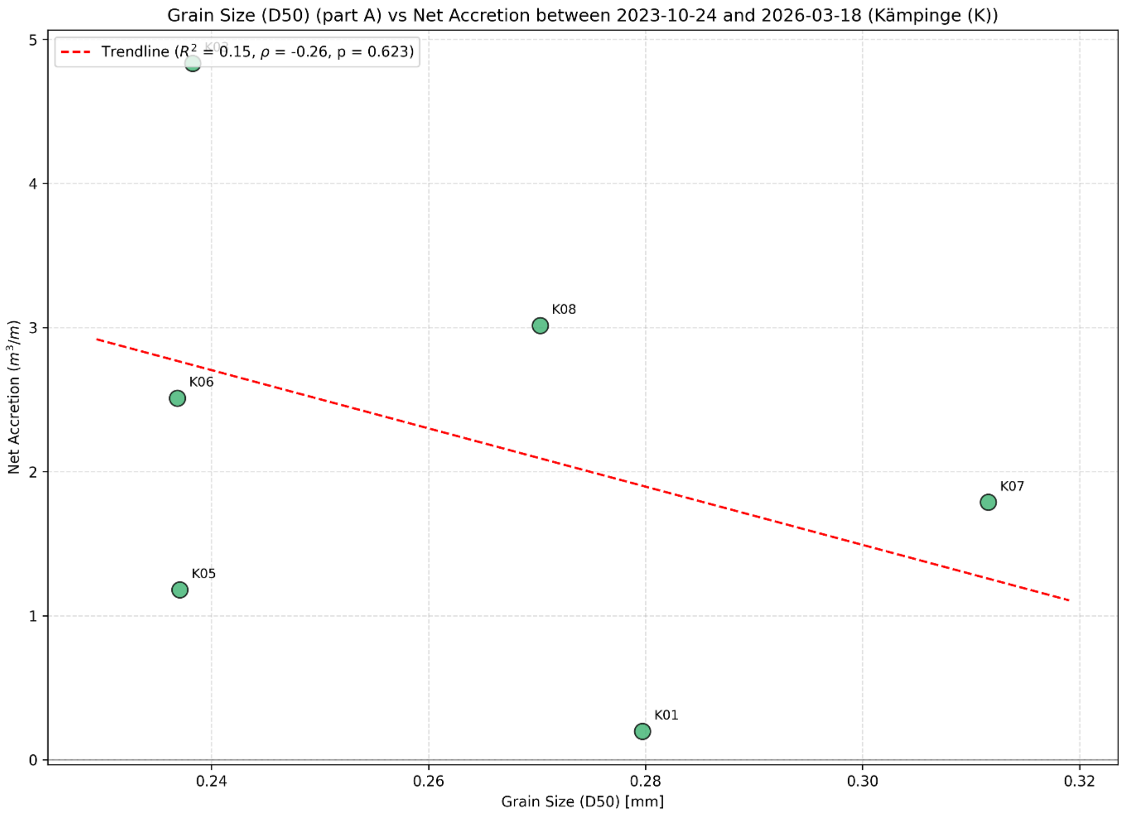

Figure A. 5: Scatter plot showing the correlation between median grain size (D50) in the swash zone (part A) and net dune accretion for Kämpinge transects.

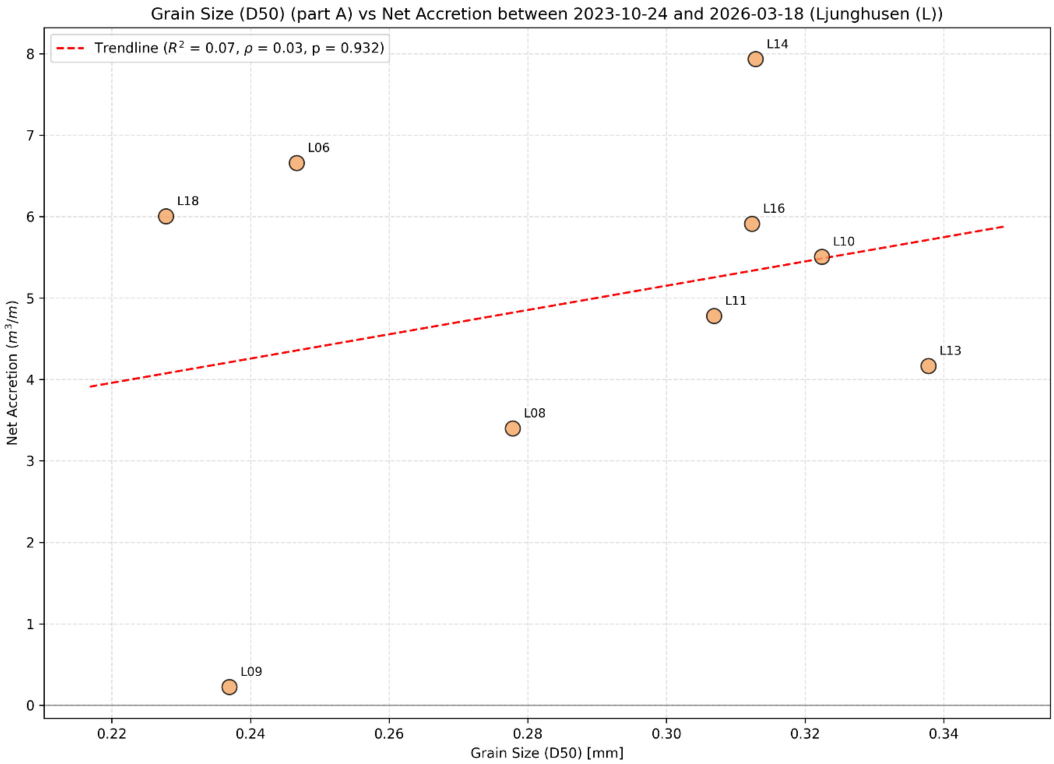

Figure A. 6: Scatter plot showing the correlation between median grain size (D50) in the swash zone (part A) and net dune accretion for Ljunghusen transects.

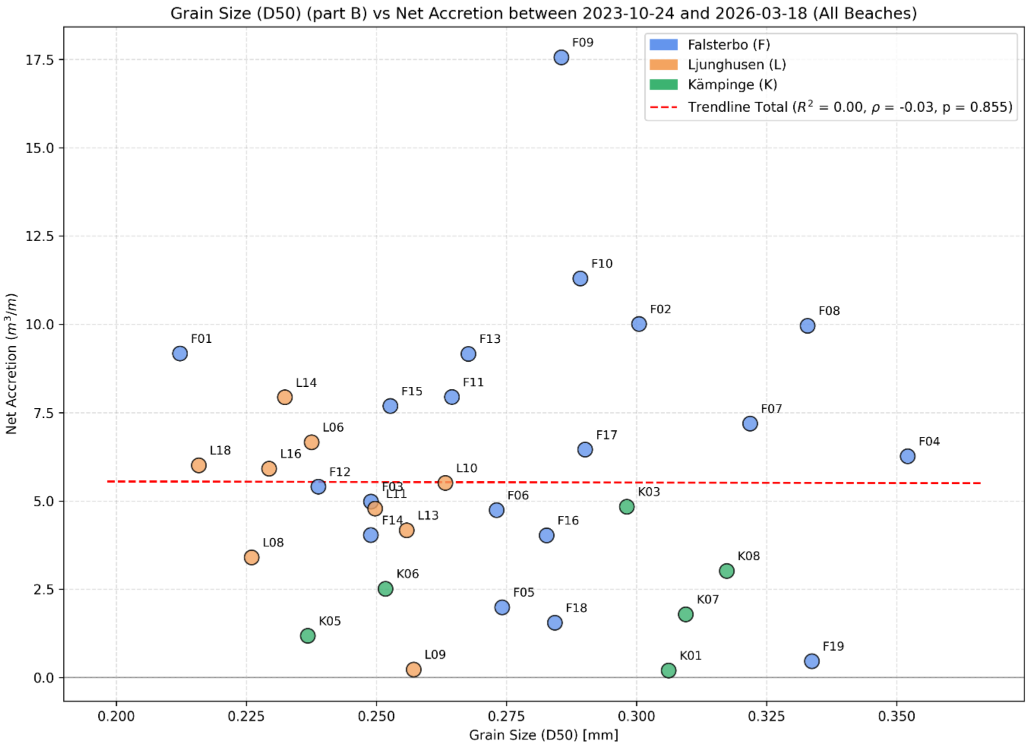

Figure A. 7: Scatter plot showing the correlation between median grain size (D50) on the mid-beach (part B) and net dune accretion across all analyzed transects.

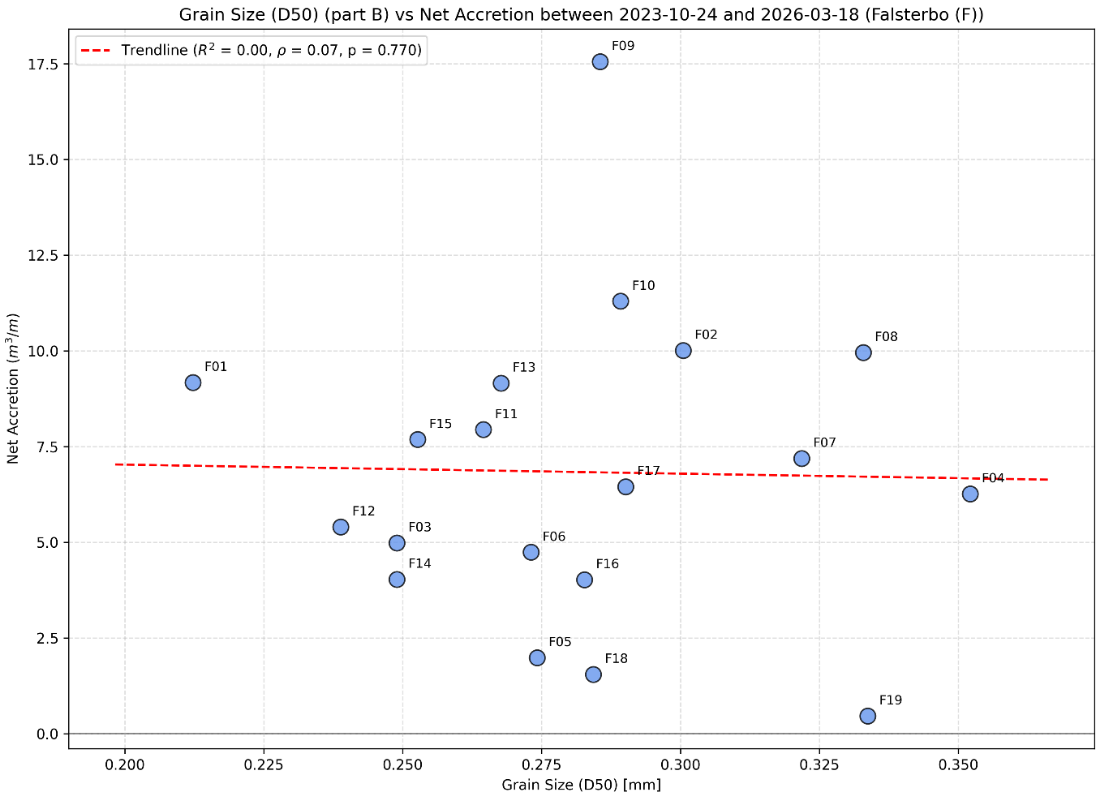

Figure A. 8: Scatter plot showing the correlation between median grain size (D50) on the mid-beach (part B) and net dune accretion for Falsterbo transects.

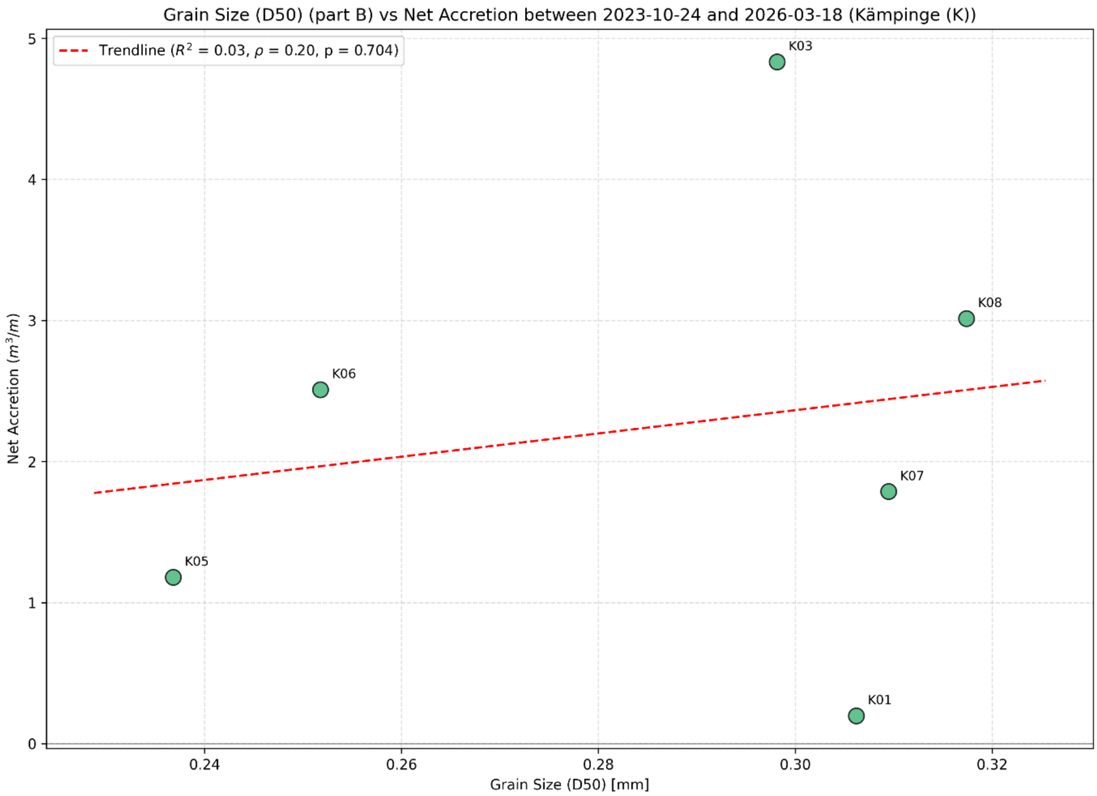

Figure A. 9: Scatter plot showing the correlation between median grain size (D50) on the mid-beach (part B) and net dune accretion for Kämpinge transects.

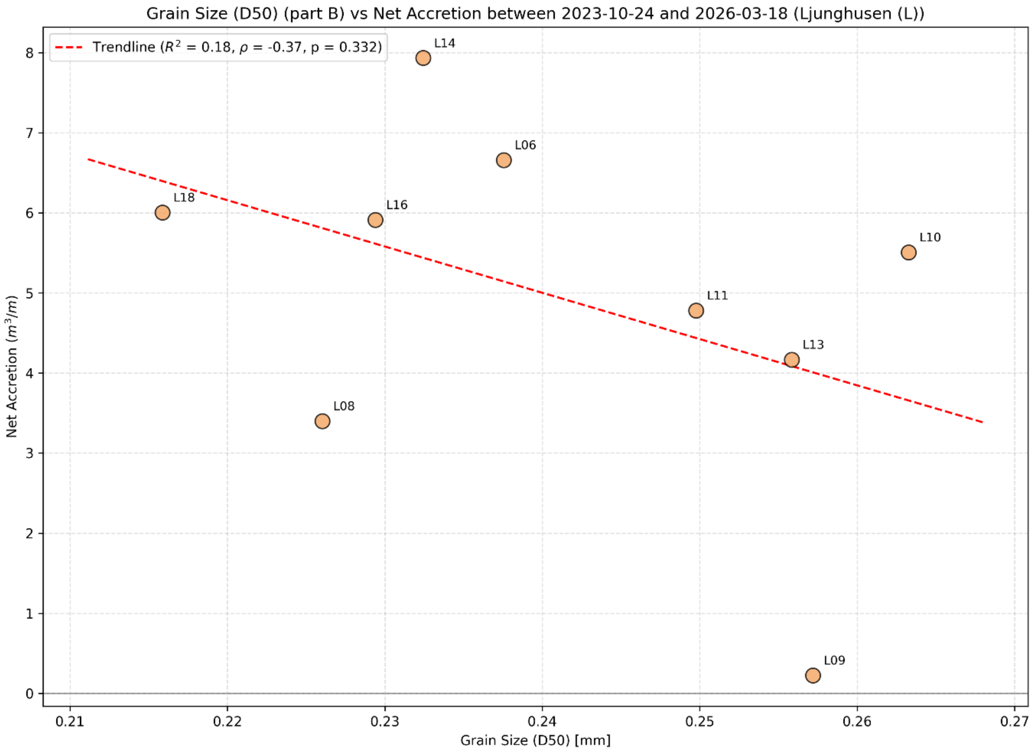

Figure A. 10: Scatter plot showing the correlation between median grain size (D50) on the mid-beach (part B) and net dune accretion for Ljunghusen transects.

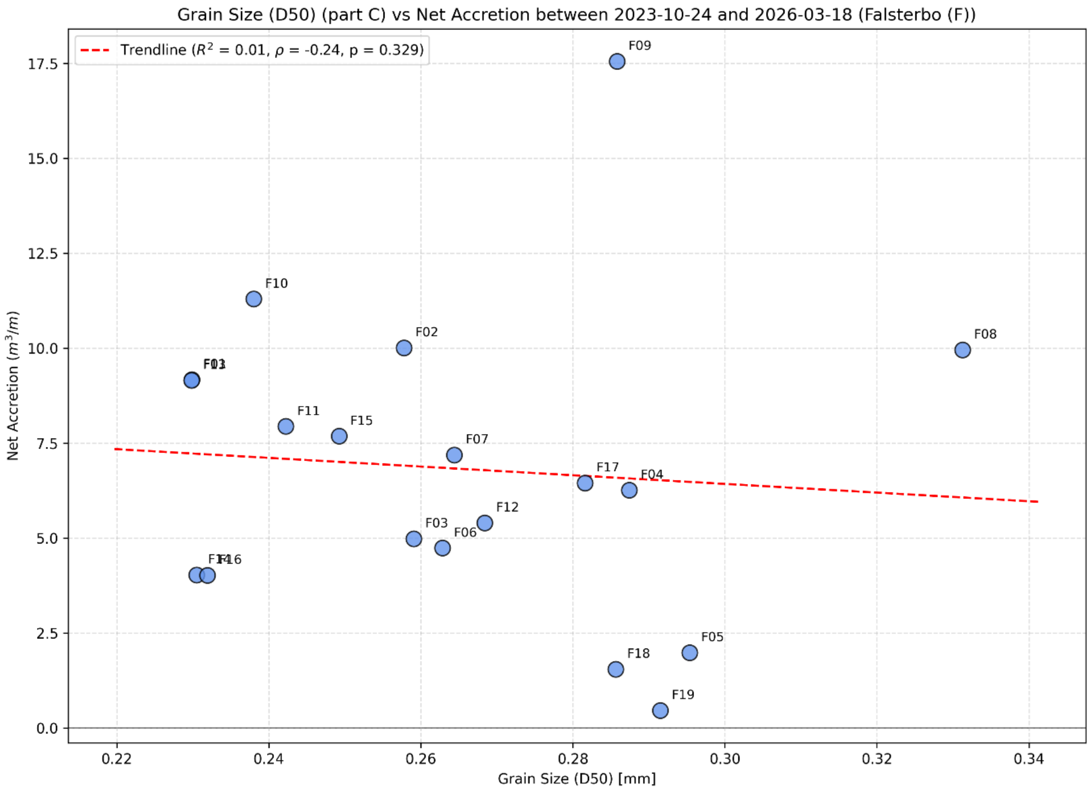

Figure A. 11: Scatter plot showing the correlation between median grain size (D50) at the dune toe (part C) and net dune accretion for Falsterbo transects.

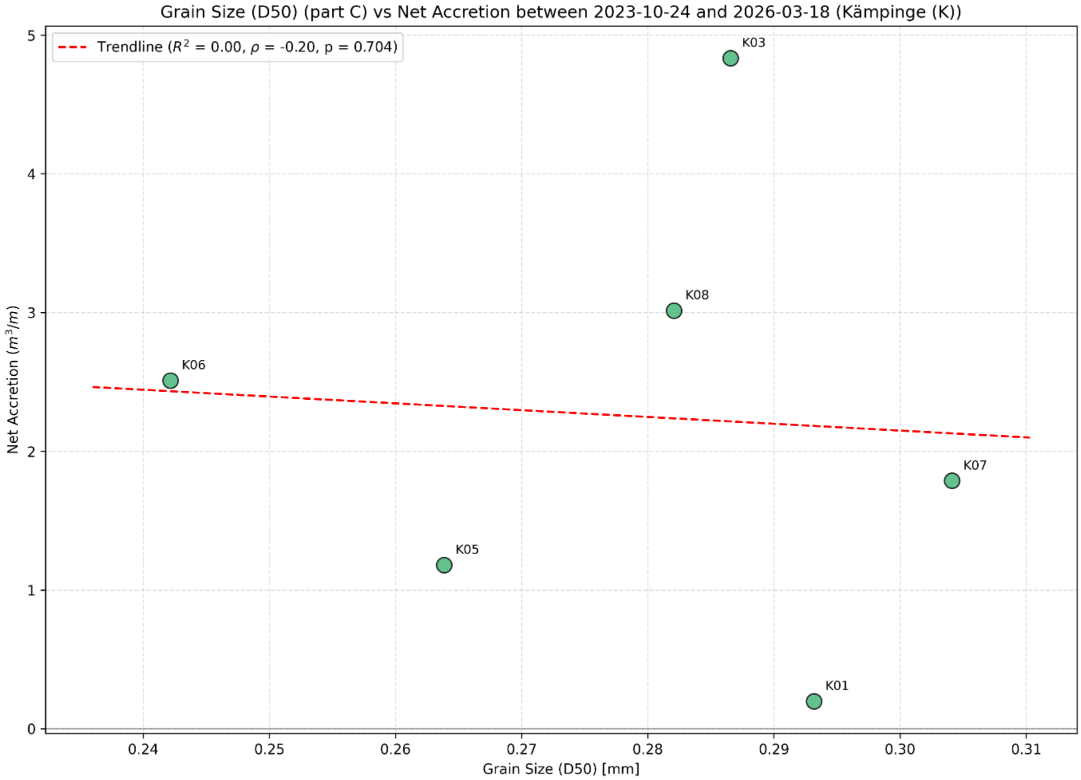

Figure A. 12: Scatter plot showing the correlation between median grain size (D50) at the dune toe (part C) and net dune accretion for Kämpinge transects.

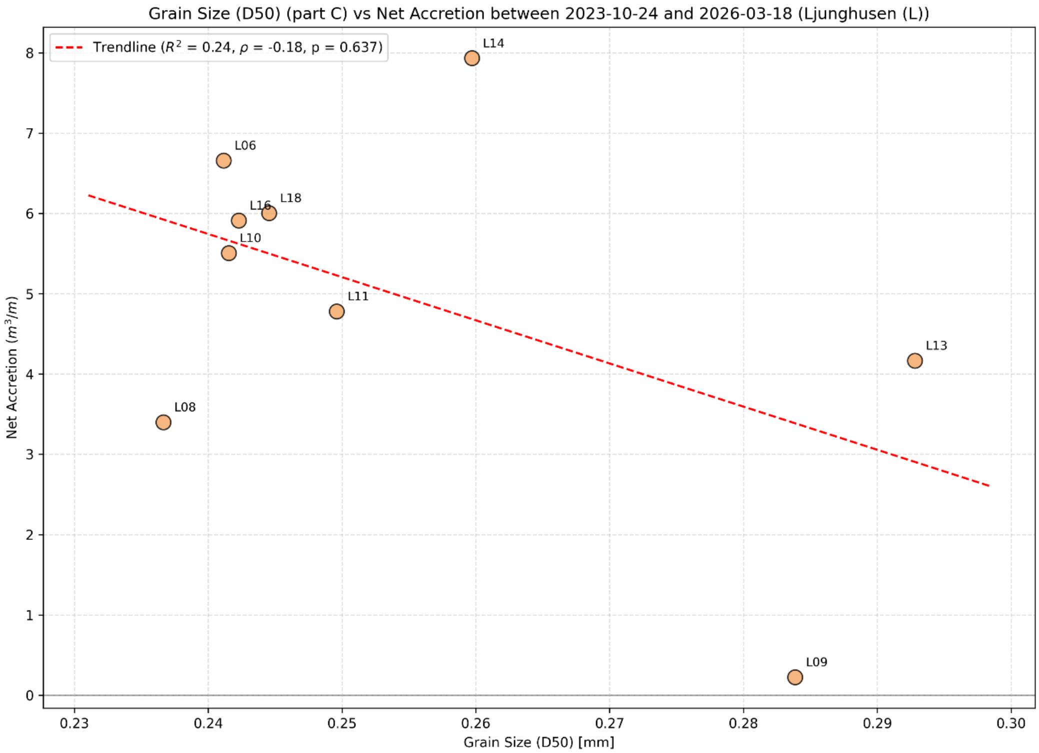

Figure A. 13: Scatter plot showing the correlation between median grain size (D50) at the dune toe (part C) and net dune accretion for Ljunghusen transects.

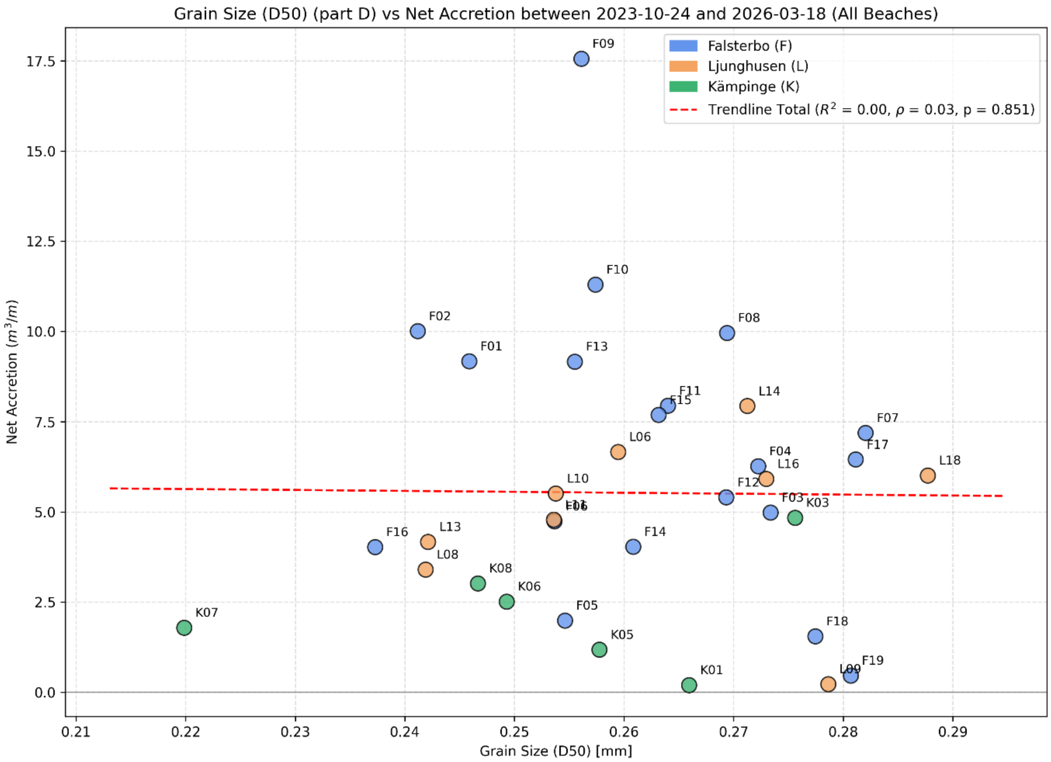

Figure A. 14: Scatter plot showing the correlation between median grain size (D50) at the dune crest (part D) and net dune accretion across all analyzed transects.

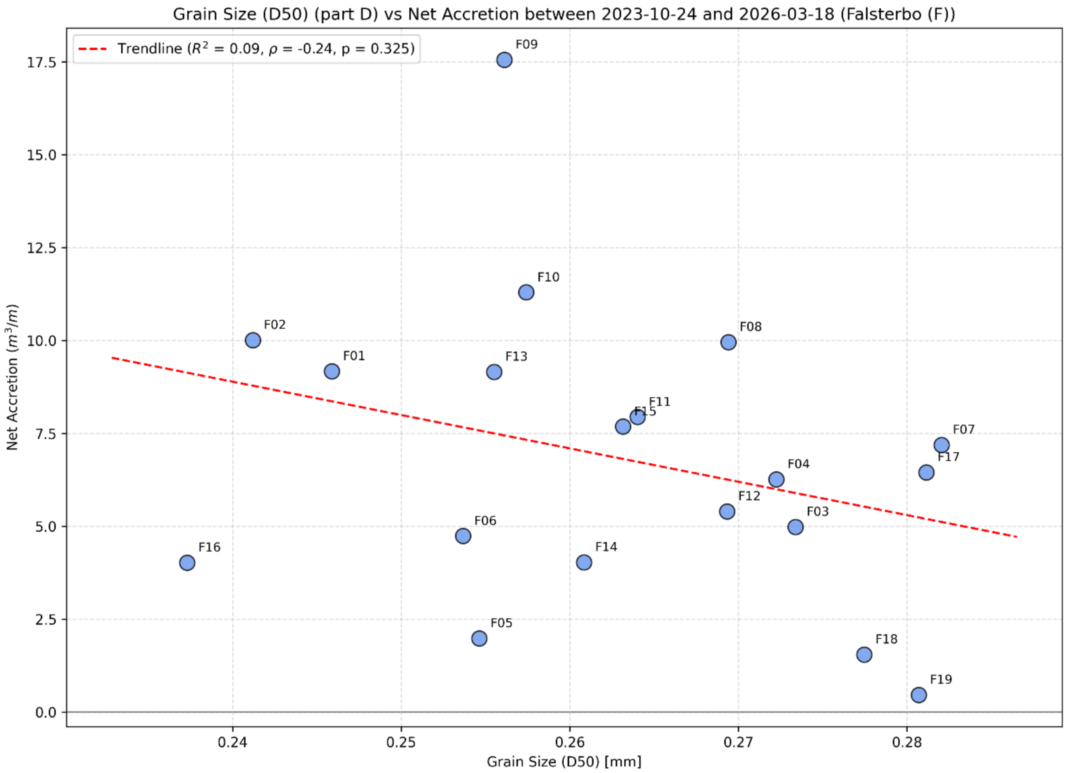

Figure A. 15: Scatter plot showing the correlation between median grain size (D50) at the dune crest (part D) and net dune accretion for Falsterbo transects.

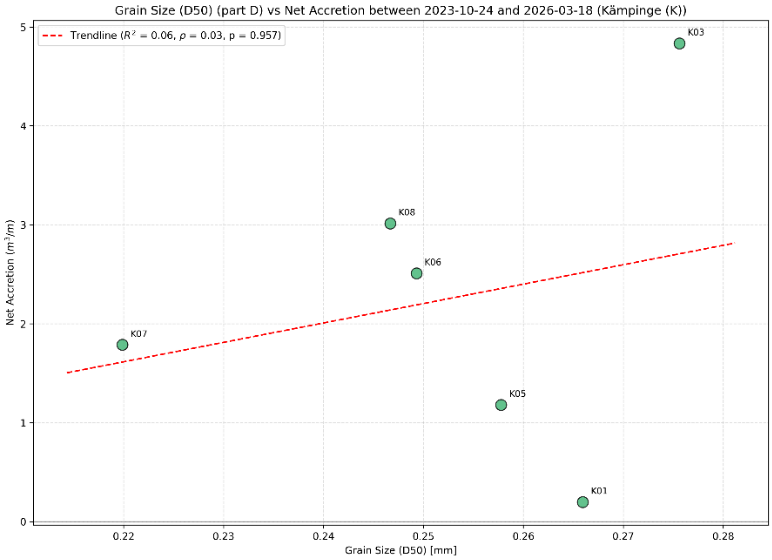

Figure A. 16: Scatter plot showing the correlation between median grain size (D50) at the dune crest (part D) and net dune accretion for Kämpinge transects.

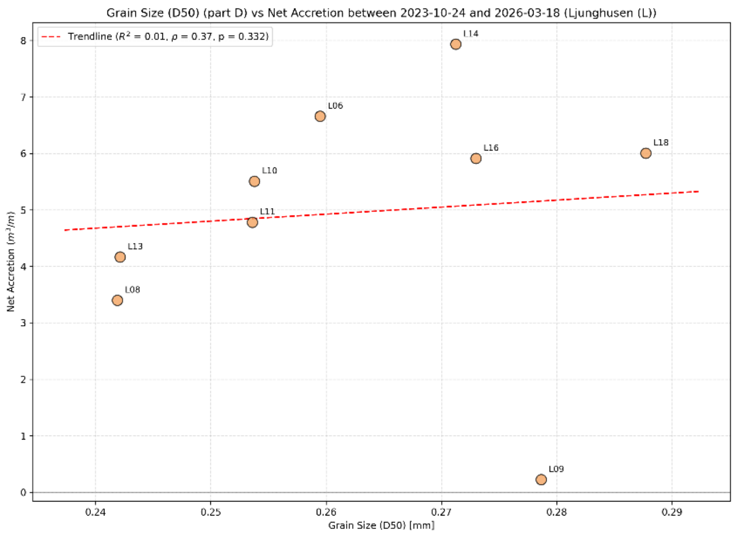

Figure A. 17: Scatter plot showing the correlation between median grain size (D50) at the dune crest (part D) and net dune accretion for Ljunghusen transects.

Table A.1: All sediment samples with weight from each sieve mesh displayed

Prov_id	2 mm	1,4 mm	1 mm	0,71 mm	0,5 mm	0,355 mm	0,25 mm	0,18 mm	0,125 mm	0,09 mm	0,063 mm	0 mm	tot
F01_A	0	0	0	0	1,1	2,6	8,9	50,2	30,3	0,7	0,1	0	93,9
F01_B	0	0	0	0	0	0,5	22,8	90,8	30	0,3	0,1	0	144,5
F01_C	0	0	0	0	0,7	3,5	42,1	74,3	14,4	0,2	0,1	0	135,3
F01_D	0	0	0	0	1	7,3	48,6	59,6	4,2	0,1	0	0	120,8
F02_A	0	0	0	0	0,3	1,2	20,4	57,8	11,8	0,2	0,1	0	91,8
F02_B	1,4	0,9	1,1	6,9	11,7	5,8	21,1	26,9	1,4	0,3	0	0	77,5
F02_C	0	0	0	0,5	2,9	8,3	47,9	48,7	3,8	0	0	0	112,1
F02_D	0	0	0	0	0,2	5,4	54,4	71,9	6,1	0	0,1	0	138,1
F03_A	2,8	0,5	1,1	14,2	28,6	11,7	20,9	14,7	1,8	0,1	0	0	96,4
F03_B	1,9	0,9	0,4	0,6	1,7	4,3	32,9	40,8	3	0	0,1	0	86,6
F03_C	0	0	0	0,6	3,2	9,2	50,4	52,9	1,7	0	0,1	0	118,1
F03_D	0	0	0	0	1,3	13,8	49,4	41,3	0,9	0,1	0,1	0,1	107
F04_A	0	0	0	0	0	0,9	25,9	59	10,5	0,3	0	0	96,6
F04_B	3,5	4,1	10,9	27,1	20	10,7	38,8	38,6	0,9	0,1	0	0	154,7
F04_C	0	0	0,5	2,8	4,6	13,3	80	43	1,2	0	0	0	145,4
F04_D	0	0	0	0	0,8	6,9	72,2	48,5	0,8	0	0	0	129,2
F05_A	2,2	2,6	7,4	22,4	9,3	6,7	39,5	31,1	1,3	0,1	0,1	0	122,7
F05_B	0	0	0,6	2,9	4,6	10,5	70,3	54,6	1,7	0,1	0	0,1	145,4
F05_C	0	0	0,7	12,9	13,2	8,9	58,8	42,5	1,2	0	0	0	138,2
F05_D	0	0	0	0,5	4	9,1	45,4	48,5	6,2	0,3	0	0	114
F06_A	0,5	0,6	1,8	8,2	16	9,1	35,2	40,6	2,7	0,1	0	0	114,8
F06_B	0	0	0	0,6	1,8	10,2	81,7	56,7	1,5	0,1	0	0	152,6
F06_C	0	0	0,4	2,8	6,4	9,8	61	61,7	3,6	0,2	0	0	145,9
F06_D	0	0	0	0	0,3	3,1	68,9	64,8	2,6	0,1	0	0	139,8

F07_A	0	0	0,6	2,9	4,7	7,7	44,3	36,3	1,4	0,1	0	0	98
F07_B	0,9	0,5	1,8	9,2	18,9	18,9	62,9	25,4	1,5	0	0,1	0	140,1
F07_C	0	0	0	0,4	1,7	5,9	73,4	59,6	1,6	0	0,1	0	142,7
F07_D	0	0	0	0,2	2,3	9,3	77	40,8	0,8	0,1	0	0,1	130,6
F08_A	0,2	0,3	0,4	1,9	2,5	3,7	40	56,9	4,7	0	0	0	110,6
F08_B	0,5	0,9	4	16	22,6	20,2	61,8	27,6	0,7	0	0,1	0	154,4
F08_C	0	0	0	5,7	28,3	28,3	79,6	18,5	0,2	0	0	0	160,6
F08_D	0	0	0	0	0	2,9	69,8	45,7	1,1	0	0	0,1	119,6
F09_A	0	0	0	0,5	0,9	2	37,9	66,2	1,4	0,1	0	0	109
F09_B	0,9	1,1	2,7	5,3	5,9	8,5	72,3	46,9	0,7	0,1	0	0	144,4
F09_C	0	0	0,1	2,3	7,1	10,9	81,5	45,7	0,6	0	0	0	148,2
F09_D	0	0	0	0	0,7	5	71,2	64	4,4	0,2	0	0	145,5
F10_A	0	0	0	0	0	0	20,6	75,9	15,1	0,4	0	0	112
F10_B	0	0	1,6	10,7	11,2	6,4	44,3	39,9	1	0	0,1	0,1	115,3
F10_C	0	0	0	0	0	0,9	44,1	65	2,2	0,1	0	0	112,3
F10_D	0	0	0	0	0	1,7	68,8	59,6	1,1	0,1	0	0	131,3
F11_A	0	0	0	0	0	0,6	33,2	62,2	7	0,1	0	0	103,1
F11_B	0,9	0	0,1	0,7	2,6	5,1	67,9	56,9	1,5	0,1	0	0	135,8
F11_C	0	0	0	0	0	2	58	74,8	1,8	0	0	0	136,6
F11_D	0	0	0	1,2	3,5	6,9	76,4	65,3	2,2	0,1	0	0	155,6
F12_A	0	0	0	0	0	1,5	48,8	65,8	1,9	0,1	0	0	118,1
F12_B	0,3	0	0,1	0,4	0,8	2,1	50,8	75,1	3,2	0,1	0	0	132,9
F12_C	0	0	0	0	0,5	3,7	67,1	46,9	0,8	0,1	0	0	119,1
F12_D	0	0	0	0	1,4	6,5	75,5	54	1,5	0,1	0	0	139
F13_A	0	0	0	0	0	0,8	36,9	67,4	4,5	0,1	0	0	109,7
F13_B	1	1,6	3,3	4,2	2,8	2,4	51,6	48,8	0,7	0	0	0	116,4
F13_C	0	0	0	0	0,8	3,1	38,4	81,4	7,7	0,1	0	0	131,5

F13_D	0	0	0	0	0,3	3,5	60,9	56,6	1,7	0	0	0	123
F14_A	0	0	0	0	0	1,4	51,8	80,2	2,4	0	0,1	0	135,9
F14_B	9,3	0,1	0,1	0,2	0,7	3	57,1	69,6	3	0	0	0	143,1
F14_C	0	0	0	0	1,3	3,6	46,5	99	7,6	0	0	0	158
F14_D	0	0	0	0,5	3,7	5,6	78,4	70,8	1	0,1	0	0,1	160,2
F15_A	0	0	0	0	0	1,3	67,1	63,6	0,5	0	0	0	132,5
F15_B	15	1,8	0,8	0,3	0,4	2,7	60,2	75,4	2,7	0	0	0	159,3
F15_C	0	0	0	0,5	0,5	3,9	68	72,2	2,2	0,1	0	0	147,4
F15_D	0	0	0	1,7	3,6	5,6	71,8	63,8	0,8	0,1	0	0	147,4
F16_A	0,1	0	0,1	0,3	0,5	1,9	43	59,2	2,9	0,1	0,1	0,1	108,3
F16_B	11,3	0,6	1,3	5,7	7,6	6	67,5	55,6	2,1	0	0,1	0,1	157,9
F16_C	0	0	0	0	0,2	1,1	46,8	90,2	4,5	0	0	0	142,8
F16_D	0	0	0	0	0	0,7	53,7	82,4	1,9	0	0	0	138,7
F17_A	0	0	0	0	0	2,7	63,2	59,5	1,3	0	0	0	126,7
F17_B	6,3	2,4	4	9,2	8	6,6	56,5	49,2	0,6	0	0	0	142,8
F17_C	0	0	0,8	2,5	2,8	10,6	78,6	47,2	0,8	0	0	0	143,3
F17_D	0	0	0	0	0,8	8	100,3	48,4	0,9	0,1	0,1	0,1	158,7
F18_A	0	0	0	0,2	0,7	4,1	58,8	66,4	0,6	0,1	0	0	130,9
F18_B	2,4	1,4	1,9	4,8	7,8	8,7	70,5	50,2	1,2	0	0	0	148,9
F18_C	0	0	0	4,7	8,4	11,4	78,1	49,3	0,3	0	0	0	152,2
F18_D	0	0	0	0	0,3	6,6	88,7	48,6	0,6	0	0	0	144,8
F19_A	0	0	0	0	0	4,1	61,4	69,4	1,6	0,1	0	0	136,6
F19_B	2,3	1	2,5	10,6	19,8	22,6	72,6	15,4	0,2	0	0	0	147
F19_C	0	0,3	1,2	3,5	4,1	10,1	98,8	39,4	0,4	0,1	0	0	157,9
F19_D	0	0	0	0	0,3	3,6	89,6	40,8	0,3	0	0	0	134,6
K01_A	0,2	0,1	0,1	0,9	6,6	18,2	48,6	37,3	9,7	0,2	0	0	121,9
K01_B	0,2	0,4	0,4	3,3	25,2	32,5	51,1	45,9	12,3	0,2	0	0	171,5

K01_C	0	0	0	1,1	7,7	22,7	70,4	36	7,7	0,3	0	0	145,9
K01_D	0	0	0	0	1,1	12,5	48,4	41,9	5,3	0,1	0	0	109,3
K03_A	0,4	0,4	0,2	0,7	2,1	8,9	41,8	57	16,5	0,1	0	0	128,1
K03_B	0	0	0	2,3	12,5	20,6	67,8	39,7	1,3	0	0	0	144,2
K03_C	0	0	0	0,5	4,3	19,5	83	43,8	5,7	0	0	0	156,8
K03_D	0	0	0	0	3	17	83,2	57,4	5,2	0	0	0	165,8
K05_A	0	0	0	0	0,8	6,7	46,1	65,8	11,9	0,2	0	0	131,5
K05_B	2,1	0,7	1,5	2,3	2,1	5,6	48,4	76,8	14,7	0,1	0	0	154,3
K05_C	0	0	0	1,1	8,4	19,8	61,4	65,3	9	0,1	0,1	0	165,2
K05_D	0	0	0	0	1,8	15,5	77,1	73,9	9,1	0	0	0	177,4
K06_A	0	0	0	0	1	6,2	37,2	58,1	8,1	0	0	0	110,6
K06_B	5,3	0,1	0,6	3,4	10,5	21,1	56,4	79,6	15,9	0	0	0	192,9
K06_C	0	0	0	0	1,4	12,3	64,5	86,7	10,7	0,2	0	0	175,8
K06_D	0	0	0	0,6	5	18,4	64,2	75,1	14,4	0,1	0,1	0	177,9
K07_A	0,2	0,8	2	3,6	18,4	19,1	47,4	29,2	6,5	0,1	0,1	0	127,4
K07_B	10,4	1,8	3,1	8,2	16,4	25,1	53,3	47	10,8	0	0,1	0	176,2
K07_C	0	0	0,4	2	18,1	33,2	100,7	43,3	7	0,3	0	0	205
K07_D	0	0	0	0	0,2	3,2	38	79,6	30	0,3	0	0	151,3
K08_A	0	0	0	0	0	3,9	81,8	49,9	4,1	0	0,1	0	139,8
K08_B	26,6	5,3	3,1	4,1	9,4	27	76,2	45,4	8,1	0,2	0,1	0,1	205,6
K08_C	0	0	0	0,3	2,1	22,3	98	51	11,5	0,1	0,1	0,1	185,5
K08_D	0	0	0	0	0,3	8,3	56,4	53,7	16,3	0,1	0	0	135,1
L06_A	0	0	0	0	0,2	3,5	48,2	52,6	3,8	0,5	0	0	108,8
L06_B	6,3	0	0,1	0	0,8	7,8	37,7	63,6	11,4	0,2	0,1	0	128
L06_C	0	0	0	0	1	10,1	39,5	54,6	9,8	0	0	0	115
L06_D	0	0	0	0	0,2	11,4	67,6	61,1	5,7	0,1	0,1	0	146,2
L08_A	1,3	0,1	0,2	0	0,1	4,7	85,1	45	1,4	0	0	0	137,9

L08_B	0	0	0	0	0	1,7	43,1	73,6	15,4	6,2	0	0	140
L08_C	0	0	0	0	0	2,3	63,5	89,2	10,3	0,3	0	0	165,6
L08_D	0	0	0	0	0	6,6	61,8	76,1	9,6	0,3	0	0	154,4
L09_A	0	0	0	0	0	3,9	47,7	61,1	13	0,2	0,1	0	126
L09_B	0,4	0,2	0,2	0,3	1,2	11,3	80,3	78,3	3,9	0,2	0,2	0,3	176,8
L09_C	0	0	0	0	0,8	18,5	65,6	40,6	2	0	0	0	127,5
L09_D	0	0	0	0	0	5,1	101,9	50,2	1	0,2	0	0	158,4
L10_A	1,3	0	0	0	2,7	40,7	77,2	15	0,4	0	0	0	137,3
L10_B	0	0	0	0	0,9	10,9	77,9	66,1	3,8	0,1	0	0	159,7
L10_C	0	0	0	0	0	3,2	66,3	82,7	6,6	0,1	0,1	0	159
L10_D	0	0	0	0	0,6	11,9	66,7	65,9	8,4	0,1	0	0	153,6
L11_A	0	0	0	0	0	19,1	86,9	11,7	0,2	0	0	0	117,9
L11_B	0	0	0	0,1	1,5	12,6	68,1	77,5	5,1	0,1	0	0,1	165,1
L11_C	0	0	0	0	0,4	9,6	73,9	79,4	5,4	0	0	0	168,7
L11_D	0	0	0	0	0	3,3	77,2	71,4	3,6	0,1	0	0,1	155,7
L13_A	0	0	0	0	3,8	45,4	43,6	19,1	0,8	0	0	0	112,7
L13_B	0	0	0	0	0,9	9,1	62,9	62,1	3,8	0	0	0	138,8
L13_C	0	0	0	0	3,3	31,4	86,1	49,2	1,4	0	0	0	171,4
L13_D	0	0	0	0	0	6,1	56	68,9	8,5	0,1	0,1	0	139,7
L14_A	0	0	0	0	6	29,5	68,5	21,9	0,1	0	0	0	126
L14_B	0	0	0	0	1,2	5,5	45,2	72,3	15,6	0,1	0,1	0,1	140,1
L14_C	0	0	0	0	0,2	11,4	84,8	75,6	5,1	0	0	0	177,1
L14_D	0	0	0	0	0	14,6	82	57,4	5,7	0,1	0,1	0,1	160
L16_A	0	0	0	0	2	33,9	73,2	21,6	0,6	0	0	0	131,3
L16_B	0	0	0	0	1,1	5,5	47,1	91,7	15,7	0,3	0	0	161,4
L16_C	0	0	0	0	1,4	10,9	60,9	82,6	8,7	0	0,1	0	164,6
L16_D	0	0	0	0	0,3	15,9	94,1	62,5	6,2	0,4	0	0	179,4

L18_A	0	0	0	0	0,7	5,7	37,6	79,9	14,6	0,1	0	0	138,6
L18_B	0	0	0	0	0	1,6	30,4	83,7	29,7	0,1	0,1	0	145,6
L18_C	0	0	0	1,2	11,5	16	54,3	82,1	13,6	0,1	0	0	178,8
L18_D	0	0	0	0	6	26	70	46,8	4,8	0,1	0	0	153,7

Table A.2: Coordinates for the location where each sediment was taken. Coordinate reference system: SWEREF 99 13 30 (EPSG:3008)

Prov_id	E	N
f01_A	106887.304	6139754.125
f01_B	106898.67	6139742.281
f01_C	106906.935	6139734.614
f01_D	106912.827	6139728.399
f02_A	107130.217	6139938.271
f02_B	107121.063	6139948.588
f02_C	107111.659	6139958.901
f02_D	107103.132	6139969.281
f03_A	107300.863	6140098.451
f03_B	107295.456	6140105.763
f03_C	107290.926	6140111.409
f03_D	107290.213	6140112.776
f04_A	107568.159	6140272.606
f04_B	107560.955	6140283.36
f04_C	107556.823	6140289.366
f04_D	107551.738	6140295.928
f05_A	107913.235	6140496.827
f05_B	107910.345	6140503.241
f05_C	107899.609	6140521.686
f05_D	107907.775	6140508.003
f06_A	108091.308	6140588.731
f06_B	108088.785	6140595.705
f06_C	108086.229	6140601.243
f06_D	108083.303	6140605.881
f07_A	108316.393	6140700.73
f07_B	108313.32	6140706.956
f07_C	108310.786	6140711.939
f07_D	108303.244	6140727.478

f08_A	108621.167	6140841.014
f08_B	108618.979	6140845.402
f08_C	108617.244	6140849.567
f08_D	108613.547	6140858.298
f09_A	108899.561	6140949.141
f09_B	108897.993	6140953.829
f09_C	108896.364	6140958.559
f09_D	108892.438	6140969.367
f10_A	109023.648	6140963.502
f10_B	109015.051	6140992.609
f10_C	109011.14	6141004.827
f10_D	109008.073	6141015.584
f11_A	109182.846	6141019.196
f11_B	109178.579	6141034.829
f11_C	109176.331	6141045.264
f11_D	109173.833	6141055.284
f12_A	109208.785	6141023.489
f12_B	109204.91	6141039.413
f12_C	109200.882	6141055.516
f12_D	109199.324	6141061.706
f13_A	109287.072	6141041.155
f13_B	109283.899	6141055.439
f13_C	109280.511	6141069.157
f13_D	109275.183	6141091.355
f14_A	109347.075	6141059.298
f14_B	109343.614	6141074.409
f14_C	109340.887	6141085.05
f14_D	109339.244	6141097.418
f15_A	109509.612	6141089.033
f15_B	109507.535	6141100.066
f15_C	109506.256	6141107.801
f15_D	109502.473	6141126.752
f16_A	109703.05	6141121.068
f16_B	109701.717	6141128.304
f16_C	109700.933	6141133.873
f16_D	109700.544	6141139.393
f17_A	109848.327	6141123.381
f17_B	109846.051	6141140.108

f17_C	109844.943	6141147.562
f17_D	109845.057	6141153.424
f18_A	109958.758	6141125.64
f18_B	109958.645	6141138.332
f18_C	109958.453	6141148.817
f18_D	109958.461	6141151.399
f19_A	110091.301	6141125.568
f19_B	110090.956	6141145.521
f19_C	110090.808	6141149.579
f19_D	110090.747	6141153.54
K01_A	115142.483	6141815.205
K01_B	115136.39	6141824.762
K01_C	115128.547	6141837.185
K01_D	115123.419	6141845.123
K03_A	115466.55	6141985.972
K03_B	115460.378	6142000.528
K03_C	115456.364	6142008.456
K03_D	115452.037	6142019.284
K05_A	115886.737	6142105.602
K05_B	115885.196	6142117.059
K05_D	115883.37	6142138.315
K05_C	115884.632	6142124.316
K06_A	116171.257	6142118.684
K06_B	116170.849	6142129.933
K06_C	116170.72	6142139.572
K06_D	116170.178	6142159.699
K07_A	116457.889	6142089.148
K07_B	116460.121	6142096.808
K07_C	116461.079	6142102.039
K07_D	116464.626	6142116.501
K08_A	116661.36	6142028.377
K08_B	116667.859	6142042.215
K08_C	116670.08	6142047.204
K08_D	116671.461	6142049.673
l06_A	113575.359	6140313.018
l06_B	113566.866	6140340.304
l06_C	113562.715	6140353.058
l06_D	113560.9	6140360.281

l08_A	113732.924	6140438.886
l08_B	113725.343	6140446.623
l08_C	113716.579	6140457.04
l08_D	113714.953	6140458.604
l09_A	113852.33	6140585.813
l09_B	113841.721	6140593.411
l09_C	113834.116	6140599.008
l09_D	113831.099	6140601.714
l10_A	113942.171	6140705.644
l10_B	113931.416	6140713.302
l10_C	113927.083	6140716.026
l10_D	113916.819	6140722.606
l11_A	114024.815	6140821.707
l11_B	114015.666	6140828.423
l11_C	114007.489	6140834.504
l11_D	114002.402	6140838.487
l13_A	114183.61	6141006.516
l13_B	114173.423	6141015.349
l13_C	114166.017	6141021.891
l13_D	114159.581	6141027.262
l14_A	114304.594	6141129.74
l14_B	114294.801	6141139.714
l14_C	114288.615	6141146.294
l14_D	114283.099	6141152.003
l16_A	114435.743	6141242.169
l16_B	114426.538	6141253.507
l16_D	114414.369	6141269.072
l16_C	114418.072	6141263.701
l18_A	114563.973	6141339.859
l18_B	114559.046	6141348.219
l18_C	114554.166	6141355.536
l18_D	114547.242	6141366.306

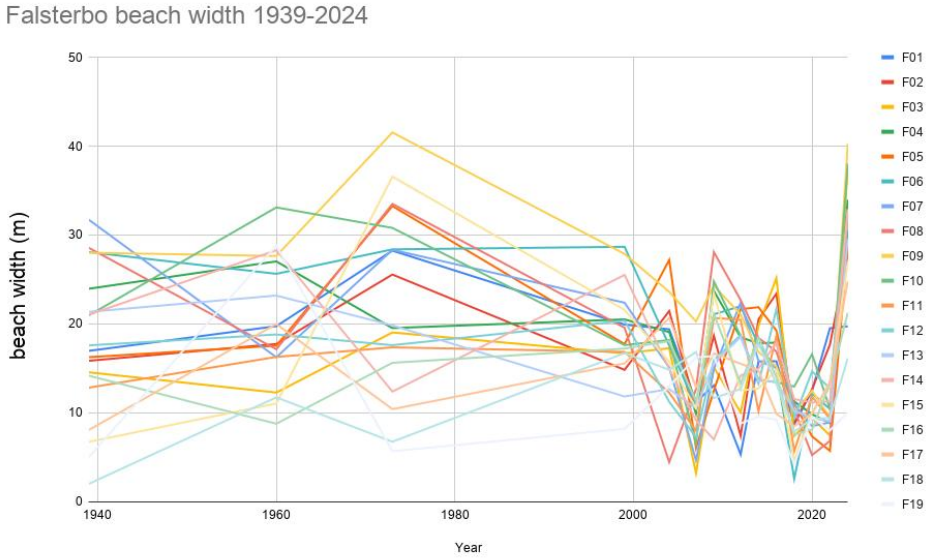

Figure A. 18: Line chart illustrating the historical changes in beach width (m) for each measured transect at Falsterbo beach from 1939 to 2024.

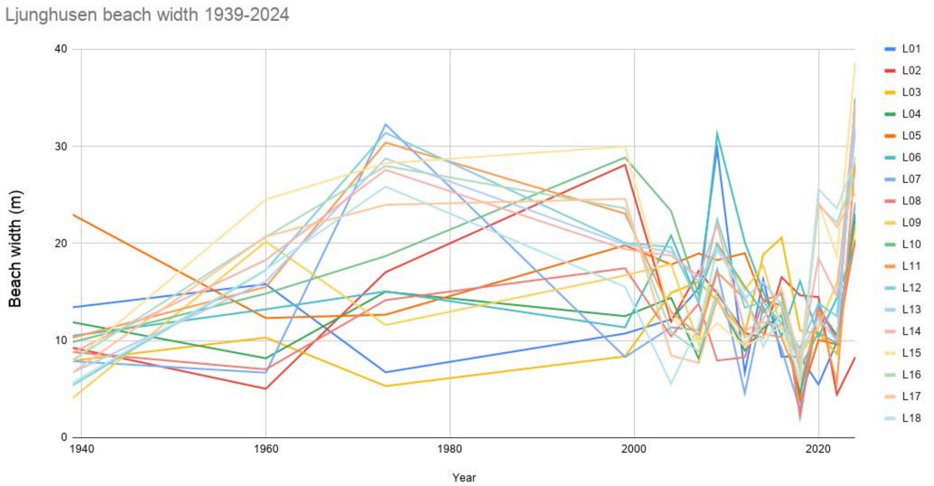

Figure A. 19: Line chart illustrating the historical changes in beach width (m) for each measured transect at Ljunghusen beach from 1939 to 2024.

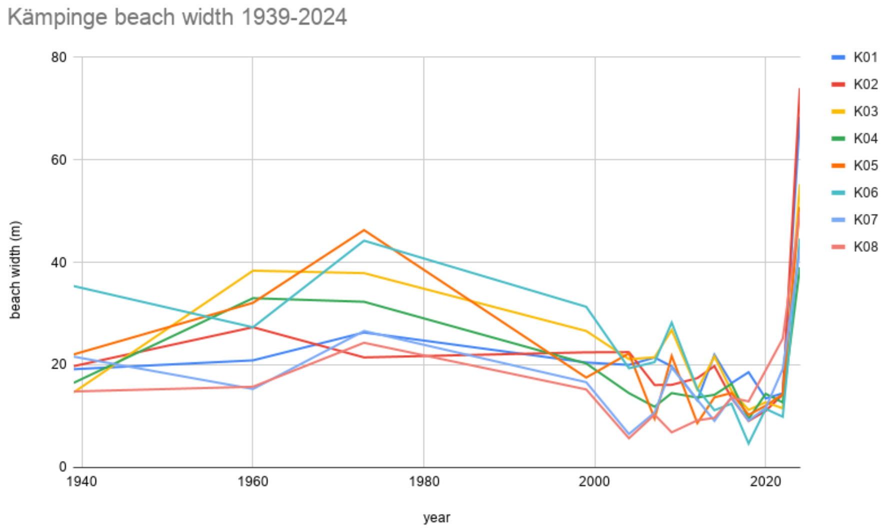

Figure A. 20: Line chart illustrating the historical changes in beach width (m) for each measured transect at Kämpinge beach from 1939 to 2024.

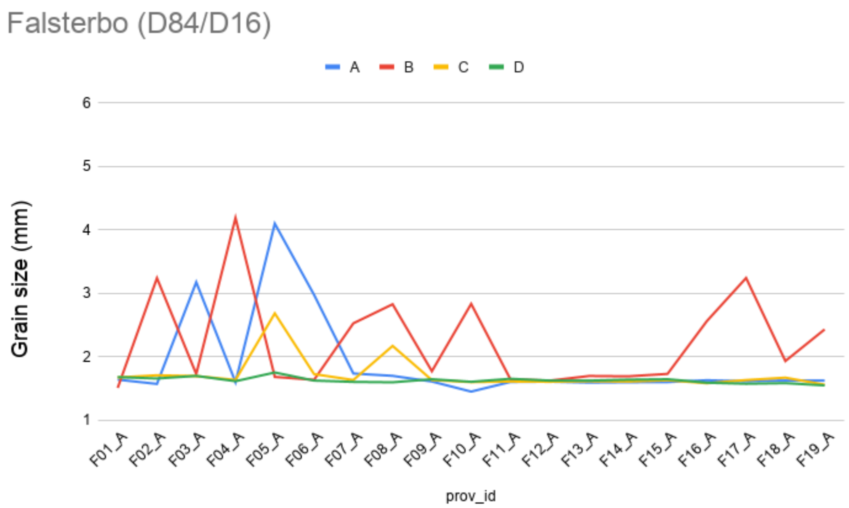

Figure A.21: Line chart showing the spatial variation in sediment sorting (D84/D16) across the four morphological zones for Falsterbo transects.

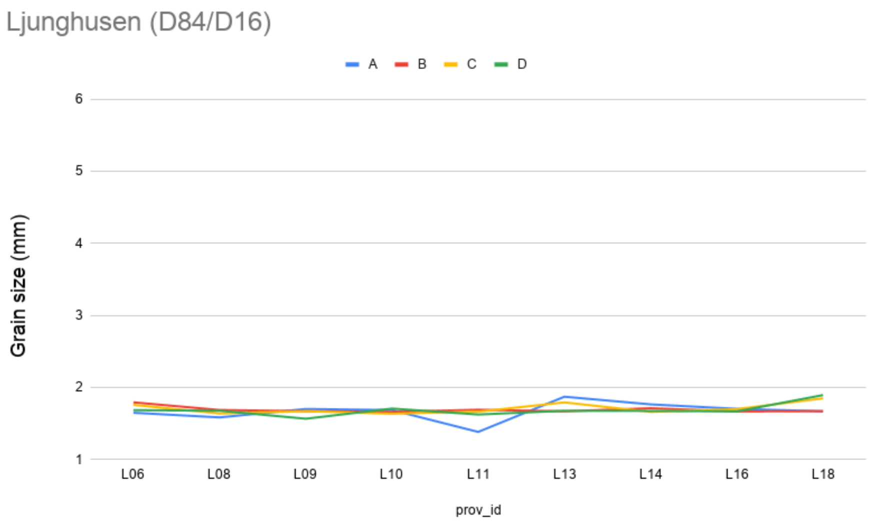

Figure A.22 Line chart showing the spatial variation in sediment sorting (D84/D16) across the four morphological zones for Ljunghusen transects.

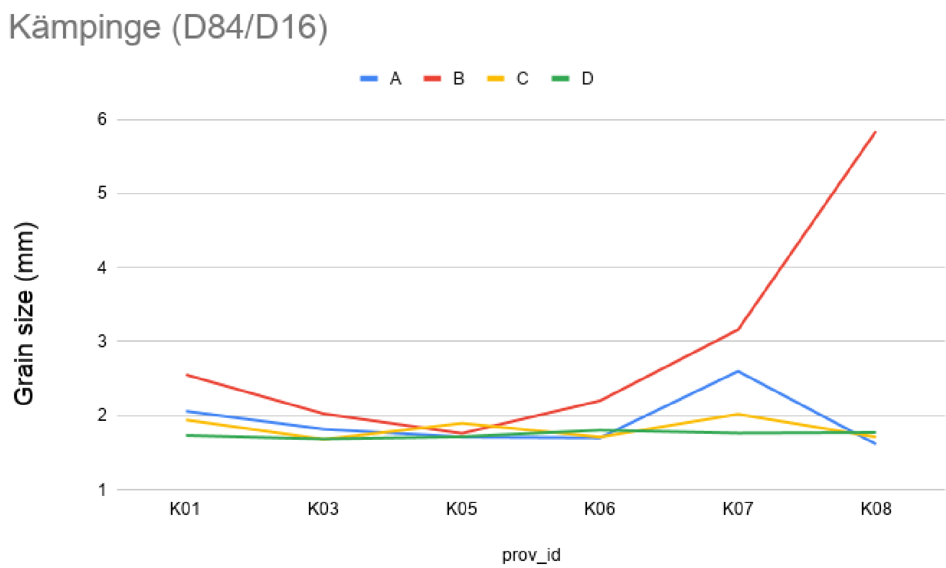

Figure A.23: Line chart showing the spatial variation in sediment sorting (D84/D16) across the four morphological zones for Kämpinge transects.